eNeuro

Research Article: New Research | Sensory and Motor Systems

Systematic analysis of transmitter co-expression reveals organizing principles of local interneuron heterogeneity

Kristyn M. Lizbinski[1], Gary Marsat[1] and Andrew M. Dacks[1]

[1]*Department of Biology, West Virginia University, Morgantown, West Virginia, 26505, USA*

DOI: 10.1523/ENEURO.0212-18.2018

Received: 28 May 2018

Revised: 7 September 2018

Accepted: 13 September 2018

Published: 21 September 2018

Author Contributions: All authors had full access to all the data in the study and take responsibility for the integrity of the data and the accuracy of the data analysis. Study concept and design: Kristyn M. Lizbinski (KML), Gary Marsat (GM), Andrew M. Dacks (AMD). Acquisition of data: KML Computational model: KML, GM. Analysis and interpretation of data: KML, GM, AMD. Drafting of the manuscript: KML, GM, AMD. Critical revision of the manuscript for important intellectual content: KML, GM, AMD. Obtained funding: AMD Administrative, technical, and material support: AMD. Study supervision: AMD.

Funding: http://doi.org/10.13039/100000055HHS | NIH | National Institute on Deafness and Other Communication Disorders (NIDCD)
R03 DC013997-01

Funding: http://doi.org/10.13039/100000181DOD | USAF | AFMC | Air Force Office of Scientific Research (AFOSR)
FA9550-17-1-0117

Funding: http://doi.org/10.13039/100000001National Science Foundation (NSF)
IOS-1557846

Conflict of Interest: The authors declare no conflict of interest.

Corresponding authors: Kristyn M Lizbinski, lizbinskik2@gmail.com; Andrew M. Dacks, PO Box 6057 Morgantown, WV 26506, tel: 304-293-3205 fax: 304-293-6363, andrew.dacks@mail.wvu.edu

Cite as: eNeuro 2018; 10.1523/ENEURO.0212-18.2018

Title: Systematic analysis of transmitter co-expression reveals organizing principles of local interneuron heterogeneity

Abbreviated Title: Transmitter co-expression heterogeneity

Authors' names: Kristyn M. Lizbinski[1]; Gary Marsat[1]; Andrew M. Dacks[1]

Institutional affiliation: Department of Biology, West Virginia University, Morgantown, WV, 26505, United States of America

Author Contributions: All authors had full access to all the data in the study and take responsibility for the integrity of the data and the accuracy of the data analysis. Study concept and design: Kristyn M. Lizbinski (KML), Gary Marsat (GM), Andrew M. Dacks (AMD). Acquisition of data: KML Computational model: KML, GM. Analysis and interpretation of data: KML, GM, AMD. Drafting of the manuscript: KML, GM, AMD. Critical revision of the manuscript for important intellectual content: KML, GM, AMD. Obtained funding: AMD Administrative, technical, and material support: AMD. Study supervision: AMD

Corresponding author(s): Kristyn M Lizbinski, lizbinskik2@gmail.com; Andrew M. Dacks, PO Box 6057 Morgantown, WV 26506, tel: 304-293-3205 fax: 304-293-6363, andrew.dacks@mail.wvu.edu

Number of pages: 40
Numbers of Figures: 8
Tables: 3
Number of words in Abstract: 250
Significance: 114
Introduction: 737
Discussion: 2649

Acknowledgements: We would like to thank Dr. Tim Driscoll and Dr. Tori Verhoeve for their advice and help with RT-qPCR experimental design and setup, Andrew Steele and Lillian Bailey for their help with cell counts and Aditya Kesari for assistance with preliminary data as well as the other members of the Dacks lab for their support. We would also like to thank Kate Allen, Tyler Sizemore, Philip Chapman, Dr. Kevin Daly, Dr. Sadie Bergeron, Dr. Quentin Gaudry and Dr. Mani Ramaswami for helpful comments on the manuscript. The TK, AST-A, and Mas-AT antibodies were provided by Dr. Jan Veenstra, the MIP antibody was provided by Dr. Christian Wegener and developed by Dr. Manfred Eckert and the FMRF antibody by Dr. Eve Marder.

Conflict of interest: The authors declare no conflict of interest.

Funding Sources: This work was supported by an R03 DC013997-01 from the NIH, and USAFOSR FA9550-17-1-0117 to AMD, as well as a National Science Foundation grant IOS-1557846 to GM.

Abstract: Broad neuronal classes are surprisingly heterogeneous across many parameters and sub-classes often exhibit partially overlapping traits including transmitter co-expression. However, the extent to which transmitter co-expression occurs in predictable, consistent patterns is unknown. Here, we demonstrate that pairwise co-expression of GABA and multiple neuropeptide families by olfactory local interneurons (LNs) of the moth *Manduca sexta* is highly heterogeneous, with a single LN capable of expressing neuropeptides from at least four peptide families and few instances in which neuropeptides are consistently co-expressed. Using computational modeling, we demonstrate that observed co-expression patterns cannot be explained by independent probabilities of expression of each neuropeptide. Our analyses point to three organizing principles that once taken into consideration allow replication of overall co-expression structure: 1- peptidergic neurons are highly likely to -co-express GABA; 2- expression probability of Allatotropin depends upon Myoinhibitory peptide expression; 3- the all-or-none co-expression patterns of Tachykinin neurons with several other neuropeptides. For other peptide pairs, the presence of one peptide was not predictive of the presence of the other and co-expression probability could be replicated by independent probabilities. The stochastic nature of these co-expression patterns highlights the heterogeneity of transmitter content among LNs and argues against clear-cut definition of subpopulation types based on the presence of *single* neuropeptides. Furthermore, the receptors for all neuropeptides and GABA were expressed within each population of principal neuron type in the AL. Thus, activation of any given LN results in a dynamic cocktail of modulators that have the potential to influence every level of olfactory processing within the AL.

Significance Statement: Understanding the functional roles of individual local interneurons (LNs) is complex because traits, like transmitter co-expression, are often partially overlapping across the population. Here, we find that single olfactory LNs co-express neuropeptides from at least four individual peptide families, and that GABA and neuropeptides are partially and heterogeneously co-expressed across the entire population. The stochastic nature of many observed co-expression patterns argues against clear-cut and exclusive definition of subpopulations based on the expression of *single* neuropeptides. Overall, our results suggest that activation of any given LN causes the release of a variable combination of neuropeptides and GABA that, based on receptor expression, target the input, output and local processing stages of the olfactory coding.

Introduction:

The historical concept of a cell-type, propelled by the work of Cajal and Golgi, suggests that distinct functional classes of neurons can be identified based on their morphology. Yet recent advances in transcriptomics and electrophysiology have revealed that even neurons within a single cell-type can still be surprisingly heterogeneous in their synaptic, biophysical and transcriptional profiles (Cohen et al., 2015; Eddine et al., 2015; Okaty et al., 2015; Li et al., 2017). Local interneurons (LNs) tend to be particularly heterogeneous across many parameters, leading to the identification of numerous LN subtypes within cortex (Flames and Marin, 2005; DeFelipe et al., 2013; Yavorska and Wehr, 2016), hippocampus (Maccaferri and Lacaille, 2003) and spinal cord (Gabitto et al., 2016; Sweeney et al., 2018). For example, two spinal interneuron populations which support different motor output (limb vs. thoracic) can be distinguished, and further subdivided, based on transcription factor expression profile (Sweeney et al., 2018).

Similarly, 13 distinct groups of GABAergic cortical interneurons exhibit partially overlapping expression of multiple neuropeptides and modulators (Gonchar et al., 2007). Thus, parameters used to classify LN sub-populations can be partially overlapping across functionally distinct sub-populations. Consequently, attempting to assign a unified functional role to sub-populations based on single molecular markers or transmitters is misleading. How then, do we reconcile heterogeneity within cell-types?

To determine the organizing principles that govern neuronal heterogeneity it is critical to use a combinatorial approach, which takes multiple parameters, like transmitter co-expression, into consideration. The insect antennal lobe (AL), analogous to the olfactory bulb, is an excellent system in which to approach this problem due to the wealth of information on local interneuron physiology, morphology and transmitter content combined with its relative numerical simplicity. The olfactory system detects and transforms odor input into meaningful output ultimately informing an animal's choice to mate, seek food, or avoid predators (Ache and Young, 2005). Odorants are first detected by olfactory receptor neurons (ORNs) which synapse onto projection neurons (PNs) within sub-structures called glomeruli that form an odor-topic map within the AL. The input/output relationship between ORNs and PNs is refined by a diverse population of LNs that transform odor information via a variety of mechanisms (Wilson, 2013). In *Manduca*, LNs are primarily inhibitory (Christensen et al., 1993), broadly tuned to odorants, exhibit both inhibitory and excitatory responses, and are highly morphologically and physiologically diverse (Hildebrand et al., 1992; Reisenman et al., 2011). However, there are no correlations between morphology, physiology and GABA expression in *Manduca* LNs (Reisenman et al., 2011) suggesting a high degree of heterogeneity within this population. Furthermore, in *Manduca*, as well as other insects, AL LNs express a combination of GABA and multiple neuropeptides

(Homberg et al., 1990; Schachtner et al., 2004; Utz et al., 2007; Utz et al., 2008; Reisenman et al., 2011; Fusca et al., 2015). Consequently, understanding the functional roles of individual LNs is complex as we lack a systematic analysis of transmitter co-expression (Nässel, 2018).

We used the olfactory system of *Manduca* to determine if sub-classes of LNs have common transmitter profiles. We characterized each pair-wise co-expression pattern for GABA and five neuropeptides, and found that although almost all peptidergic LNs co-express GABA, neuropeptide co-expression is heterogeneous across LNs. Using computational modeling, we demonstrate that many co-expression patterns cannot be explained by independent probabilities of expression of each peptide, highlighting that certain pairs of peptides co-occur more (or less) often than by chance. For other pairs, the presence of one peptide was not predictive of the presence of the other, and co-expression probability could be replicated by independent probabilities. The stochastic nature of these co-expression patterns highlights the heterogeneity of transmitter content among LNs and argues against clear-cut and exclusive definition of subpopulation types based on the presence of a *single* neuropeptide. One possible explanation for this heterogeneity is that principal cell classes within the AL express different GABA and neuropeptide receptors. This would segregate the influence of each modulator across different cell types (Nusbaum et al., 2001; Tritsch et al., 2016; Nusbaum et al., 2017) as is the case for the clock network of *Drosophila* (Liang et al., 2017). However, this is not likely to be the case here, as all neuropeptide and $GABA_B$ receptors were expressed within every cell class of the AL (ORNs, PNs and LNs). Overall, our results suggest that activation of any given LN likely releases a variable combination of peptides and GABA to potentially influence every cell class within the AL.

Materials and Methods:

136 *Animals*: *Manduca sexta* were raised at West Virginia University as previously described (Bell
137 and Joachim, 1976; Daly et al., 2013). Equal numbers of unmated adult males and female moths
138 were pooled for all data.
139 *Immunocytochemistry:* Brains were dissected in physiological saline (Christensen and
140 Hildebrand, 1987), fixed in 4% paraformaldehyde overnight at 4°C, embedded in 5% agarose to
141 be sectioned at 100µm using a Leica VT 1000S vibratome. Sections were washed in PBS with
142 1% triton X-100 (PBST), blocked in PBST and 2% IgG free BSA (Jackson Immunoresearch;
143 Cat#001-000-161) and then incubated in blocking solution with 5mM sodium azide and primary
144 antibodies. For all rabbit-neuropeptide/mouse-GABA protocols, sectioned tissue was incubated
145 for 48 hours at dilutions of 1:3000 and 1:500 respectively. Sections were then briefly washed
146 with PBS, PBST, cleared with ascending glycerol washes and then mounted on slides with
147 Vectashield (Vector Laboratories; Cat#H-1000). All neuropeptide antibodies used in this study
148 were raised in rabbit. For protocols in which we labeled with two antisera raised in rabbit, we
149 used APEX Antibody Labeling Kits 488, 555, 647 (Invitrogen;Cat #s A10468, A10470, A10475,
150 respectively) to directly attach a fluorophore with excitation/emission spectra at different
151 wavelengths to each primary to avoid cross-labeling from a secondary antibody (Bradley et al.,
152 2016). Using the resin tip from the APEX kit, a small amount of the antibody (10-20µg) was
153 pushed through the resin using an elution syringe and the reactive dye was prepared using
154 DMSO and a labeling buffer (Solutions provided in APEX kit). The reactive dye was eluted
155 through the tip onto the antibody remaining in the resin to covalently bond the fluorescent label
156 to the IgG antibodies. The tip was incubated overnight 4◦C or at room temperature for 2 hours
157 and the labeled product was eluted through the tip. Resulting labeled antibody volume of 50uL in
158 a total volume of 2400ul was used to label 6 brains at equal dilution of 400ul per well and

incubated for 72 hours in 3% triton X-100 with PBSAT. Sections were then washed and mounted as above.

Antibody Characterization: Specificity controls (including pre-adsorption controls) for the AST-A, Mas-AT, TK, and MIP antibodies in *Manduca* brain tissue are described completely in (Lizbinski et al., 2016). GABA pre-adsorption controls in *Manduca* AL tissue for the mouse GABA antiserum are described in (Bradley et al., 2016). The antibodies used in this study likely cross-react with several isoforms within the same peptide family. Thus, our results can only resolve principles at the level of peptide family and not individual peptide isoforms.

GABA- The GABA antibody (Sigma Aldrich, cat # A2052) was raised in rabbit against GABA coupled to BSA with paraformaldehyde.

MIP- Antiserum raised in rabbit against MIP conjugated to thyroglobulin was produced by M. Eckert, Jena Germany and provided by C. Wegener, Marburg Germany (Predel et al., 2001). (RRID: AB_2314803).

Mas-AT -Antiserum raised in rabbit against *Manduca* allatotropin (Mas-AT) was kindly provided by Dr. J. Veenstra, University of Bordeaux, Talence, France; (Veenstra and Hagedorn, 1995). (RRID: AB_2313973)

AST-A- Antiserum was raised (Reichwald et al., 1994) in rabbit against octadecapeptideallatostatin (Pratt et al., 1991), ASB2, (AYSYVSEYKALPVYNFGL-NH2) of *Diploptera punctata* and kindly provided by Dr. J. Veenstra, University of Bordeaux, Talence, France. It recognizes AKSYNFGLamide, a form of AST and other AST-like peptides.

TK- Antiserum raised in rabbit against locust tachykinin II with bovine thyroglobulin with glutaraldehyde was kindly provided to us Dr. J. Veenstra, University of Bordeaux, Talence, France. (RRID: AB_2341129)

FMRF- FMRFamide antiserum was raised against synthetic RF-amide coupled to bovine thyroglobulin with glutaraldehyde and provided by Dr. Eve Marder (Marder et al., 1987). Pre-adsorption controls of the antiserum against synthetic FMRFamide eliminated labeling in larval *Manduca* nervous tissue (Witten and Truman, 1996).

Confocal Microscopy: Image stacks were scanned using an Olympus Fluoview FV1000 confocal microscope with argon and green and red HeNe lasers. Scans were taken at either 800x800 or 1024x1024 pixel resolution, 1.5 um between optical sections, using both 20x/0,80 Oil UPlanApo and 40x/1.30 Oil ∞ 0.17/FN 26.5, 80um pinhole size, Olympus lenses. Fluoview (FV10-ASW Viewer software(Ver.4.2b)) was also used to set brightness levels and Corel Draw X4 was used to organize figures.

Cell counts and co-expression: Images of immunostained brains were exported as .tiff stacks in Fluoview software. Stacks were then imported into VAA3D software (available at www.vaa3d.org/) (Peng et al., 2010) to determine individual cell counts and co-expression cell counts. The number of local interneurons in the lateral cell cluster that express each transmitter were counted in VAA3D (n=6 brains per label combination, 3 brains per sex). We used cell body size, and location within the lateral cell cluster to distinguish between LNs and PNs (Homberg et al., 1988). The average and standard deviation of number of cells per AL that expressed a given transmitter were calculated for each combination. Wilcoxon rank sum tests were performed using Graph Pad Prism v.5.01 (Graphpad Software Incorporated) to determine if there was any significant difference between the left and the right AL for each brain. Co-expression ratios were determined by dividing the number of cells expressing both an individual neuropeptide and

GABA by the total number of cells expressing just the neuropeptide and calculated in Excel. Neuropeptide co-expression ratios were determined in the same manner for every possible pairwise combination using data from peptides stained using the APEX kits. FMRF/MIP co-expression ratios were not calculated as the APEX kits labeled significantly less MIP neurons than all other runs and therefore the ratios would not have reflected accurate co-expression. Thus, FMRF/MIP co-expression was not used in subsequent models or computational analysis as neither a constraint nor a relationship to replicate. All other neuropeptide/neuropeptide co-expression experiments labeled an accurate # of cell bodies when compared to cell counts from GABA/neuropeptide runs using indirect immunocytochemistry. Cell count totals and standard deviations from APEX kit labeling (Figure 2) were used in all model iterations, as co-expression ratios were calculated using that data.

Putative neuropeptide receptor sequence BLAST: We used receptor sequences from closely related invertebrate species to identify putative sequence homologs on *Manduca* scaffolds. Protein sequences from *Drosophila melanogaster* and other closely related species were identified by annotation (see Table 2) and queried against the *Manduca* genome using tblastn (National Agricultural Library, i5k initiative https://i5k.nal.usda.gov/Manduca_sexta). Top matches to each receptor sequence in *Manduca* were subsequently queried against the NCBI nr database to confirm their putative annotation as *Manduca* receptor homologs. These sequences were used for primer design for RT-qPCR analysis of putative neuropeptide receptor expression in the antennae, medial and lateral cell clusters, and brain. Sequences that were previously identified in *Manduca* for Mas-ATr and RpS3 (Jiang et al., 1996; Horodyski et al., 2011) were downloaded as FASTA files from NCBI (http://www.ncbi.nlm.nih.gov/gene/?term=) and used to

design RT-qPCR primers. Open reading frames were established using ORF Finder at http://www.ncbi.nlm.nih.gov/projects/gorf/. A recent study partially annotated the *Manduca* genome (Kanost et al., 2016). We used the *Manduca* raw sequence, and assembled genome sequence at NCBI Assembly ID GCA_000262585 from Kanost (http://www.ncbi.nlm.nih.gov/assembly/GCA_000262585.1) (Kanost et al., 2016) and identified the sequence IDs for each of the transcripts in question (Table 1). None of the putative receptor sequences are currently annotated in NCBI Assembly ID GCA_000262585.

Primer design: Open reading frame nucleotide sequences for each receptor, as established above, were used as the basis for primer design for RT-qPCR. Primers were designed using http://www.bioinformatics.nl/cgi-bin/primer3plus/primer3plus.cgi and checked for optimal conditions using OligoAnalyzer 3.1 (https://www.idtdna.com/calc/analyzer). Primers and amplicons were then run through a BLAST of the *Manduca* genome to determine if they matched to the specified sequence and to rule out potential priming mismatches with other parts of the genome. Table 2 lists primer sequences and annealing temperatures. All primers used for RT-qPCR amplified a 90-125bp stretch of sequence.

Real Time (RT) qPCR: Antennae, medial cell clusters, lateral cell clusters and brains were collected from 2-6 day old, unmated, naive adult *Manduca* and RNA was extracted using a TRIzol reagent (Molec. Research center Cat# # TR 118). Equal numbers of pooled males and females were used for each biological tissue sample for a total of 3 biological samples for each tissue type (n=3 antennae; n=40 medial cell clusters from 20 brains; n = 40 medial cell clusters from 20 brains; and n= 2 brains). We used the 40s ribosomal protein s3 (RpS3) as our reference

gene. RpS3 expression values were consistent across biological replicates. RNA was treated with TURBO DNA-free™ Kit (ThermoFisher Scientific Cat# AM1907) to prevent genomic DNA contamination and cDNA was synthesized using the SuperScript® IV First-Strand Synthesis System (ThermoFisher Scientific Cat#18091050). We performed RT qPCR with the BioRad CFX Connect Real-Time System (Cat #1855201) to determine the relative expression of putative neuropeptide receptors across our tissue samples. Individual samples were prepared by combining prepared cDNA sample, [100um] forward and reverse primers, SsoFast EvaGreen Supermix (BioRad Cat # 1725200) and nuclease free diH_20 to a volume of 10ul. RT^- samples, no template controls (NTCs) and positive controls with *Manduca* genomic DNA from the brain were run for every plate. RT^- and NTC had no amplification for all receptors and sample types run at 58.3˚C (See Table 3). Optimal annealing temperatures were determined through a gradient test on genomic DNA to ensure qPCR on cDNA was performed at optimal temperature. All primer sets, including the reference gene, RpS3, were run using the following protocol (95^oC 2 minutes, (95^oC 5 seconds-> 58.3^oC 30 seconds) x 39 cycles, 65.0^oC 5 seconds stepped up to 95^oC) except for Mas-ATr primers, which were annealed at a temperature of 52^oC. All samples for RpS3 were run again at 52˚C to ensure accurate calculation of relative expression values for Mas-ATr. Cq values for ANTa (antennae sample a), Mb (Medial cell cluster sample b) and NTC sample for the RpS3 run at 52˚C were high (see Table 3). However, amplification curves revealed that there were no sharp amplification peaks and thus, high Cq values were due to noise not contamination. High Cq values with non-descript peaks for RpS3 NTCs run at 52˚C were considered 0 for ANTa, Mb and NTC when calculating relative expression.

qPCR relative expression analysis: Raw qPCR data can be found in Table 3. Delta Ct ($Ct_{receptor}$-$Ct_{reference\ gene}$) values were calculated for each receptor using RpS3 Ct values as the reference gene, and averaged across all biological replicates for brain, lateral cell cluster, MCC and antennae tissue samples. Relative expression levels ($2^{-\Delta CT}$) were calculated for all receptors. Ct values less than or equal to 37 were considered non-detectable. All graphical representations for receptor qPCR were performed in GraphPad prism (v. 5.01).

Computational analysis of transmitter co-expression: We wrote a MATLAB (Naticks MA) program to determine if our observed transmitter co-expression data could be replicated by independent probabilities of expression of each transmitter. Given the known total number of LNs in the lateral cell cluster, and the total number of LNs expressing each neuropeptide from our cell counts, the model determines the probability of a given neuron co-expressing two transmitters. The program is given the average number of cells expressing a given neurotransmitter and then randomly assigns them to one of the cells in the cluster. The model can thus determine the probability of pairwise co-expression (i.e. 100% of TK cells express MIP) in the lateral cell cluster based on chance. Specifically, using our observed data as the backbone of the model, we designed a matrix with 6 columns, 1 per transmitter type (TK, FMRF, Mas-AT, MIP, AST-A, GABA), with a row length of 360 long (the total number of LNs in the lateral cell cluster) (Homberg et al., 1988). Within each column, the model randomly distributes the number of cells that express a given transmitter to a row between 1 and 360 (Fig. 3A). For example, if we know that 12 cells within the lateral cell cluster are TKergic, the model randomly picks 12 numbers between 1 and 360 in the TK column, and marks that cell as TK positive. The number of cells expressing a certain neurotransmitter is chosen probabilistically based on the observed

296 average and standard deviation of the number of neurons that express a given transmitter. With
297 each iteration of the model, the cells that are assigned as 'transmitter positive' within each
298 column are randomized. The model does this with all respective cell count totals for each
299 transmitter column and then calculates the percentage each transmitter is expressed with another
300 transmitter based on independent expression of each transmitter (across all pairwise
301 comparisons). Standard deviation and percentages of co-expression were recorded across 10,000
302 iterations of the model. We then compared our observed co-expression percentages to the
303 model's output to determine if independent probabilities of expression of each transmitter could
304 explain observed co-expression.
305
306 The model described above has no initial assumption about the likelihood of co-expression and
307 only the overall number of cells expressing each of the transmitter is determined initially. We
308 used a similar model to determine if assigning dependent co-expression relationships for specific
309 pairs of transmitters could replicate the co-expression patterns for other transmitter pairs. To do
310 this, we built certain co-expression relationship explicitly as initial assumptions. For example, if
311 we know that on average 100% of TKergic cells are also MIPergic, the program explicitly forces
312 100% of the cells that are assigned to be TK positive to also be MIP positive. This co-expression
313 relationship is thus no longer determined based on independent expression probabilities like the
314 first version of the script, but rather is an initial assumption – a rule. We can then determine if
315 this rule alone shifts the co-expression of other transmitter types closer to the observed co-
316 expression percentages. We applied these rules one by one (for a total of 92 different models),
317 for every pairwise comparison of co-expression and statistically compared the output of the
318 independent expression model to the output of the rule based model as well as the observed co-

319 expression patterns we identified with immunocytochemistry. This allowed us to determine if
320 specific co-expression relationships could replicate other co-expression relationships within LNs.
321 The script was run on a Windows 7 desktop, with an Intel ® Core™ 17-3770 CPU @ 3.4GHz
322 processor, and a 64-bit operating system.
323
324 *Code Accessibility*: Custom MatLab scripts available at [URL redacted for double-blind review], at
325 [URL redacted for double-blind review], or upon request. The code is available as Extended Data.
326
327 *Experimental Design and Statistical Analysis:* The model outputs a predicted percentage of co-
328 expression for every pairwise co-expression relationship. To statistically determine how well the
329 model replicated observed co-expression %s, we used standard deviation indices (SDIs) to
330 determine how close the model's predicted co-expression % is to observed probability of co-
331 expression. Similar to a Z-score, this measure is calculated as follows:
332 $SDI = (Mean_{model} - Mean_{observed}) / stdev_{greatest}$
333 Where $Mean_{model}$ = Mean probability of co-expression of any two given neurotransmitters from
334 the model e.g. mean % TK co-expressed with MIP
335 $Mean_{observed}$ = Mean probability of co-expression of any two given neurotransmitters from the
336 observed co-expression relationships
337 $stdev_{greatest}$ = the greatest standard deviation from either the model or observed data for a given
338 co-expression relationship.
339 Weighted SDI's were calculated to reflect the match between data and model for the overall
340 population of LN by weighting the contribution of each neurotransmitter proportionally to its
341 prevalence.

342 Weighted SDI = $\sum$ (($Mean_{model} - Mean_{observed} / stdev_{greatest}$)*($n_{co\text{-}expressed} / n_{total}$)

343 For example, there are only 12 TK neurons in a total of 360 LNs, but 142 Mas-AT neurons.
344 Therefore, predicting the number of Mas-AT neurons vs. TK neurons should carry more weight
345 when determining the accuracy of each model. Weighted SDIs for each co-expression
346 relationship (i.e. weighted SDI for the TK/MIP co-expression) were summed across relationships
347 for an overall measure of the accuracy with which each model iteration replicated observed co-
348 expression patterns.

349 SDI values can be interpreted by the following scale: 0: perfect consensus between model and
350 experimental data; 1: model results are within one standard deviation of experimental data and
351 thus replicate the data reasonably well; 2: model results are within two standard deviation of
352 experimental data and thus do not replicate the data accurately. To determine the % improvement
353 of each model at replicating observed co-expression (Fig 3G), all weighted SDI's were
354 normalized with respect to the weighted SDI of the independent expression model using the
355 formula:

356 % improvement from "independent-expression" model = (1-(weighted SDI_x/ weighted
357 SDI_{ind}))*100

358 All statistics were performed in GraphPad prism (v. 5.01).

359 ***Results*:**

360 The antennal lobe (AL) of *Manduca* is surrounded by 3 cell clusters that house the cell
361 bodies of projection neurons and LNs. The lateral cell cluster consists of ~950 cell bodies,
362 including 590 projection neurons and ~360 total LNs (Homberg et al., 1988), of which ~170 are
363 GABAergic (Hoskins et al., 1986). *Manduca* LNs are diverse across several traits with no

correlations between physiological properties, morphological properties, or GABA expression patterns in LNs (Reisenman et al., 2011). We therefore took a systematic approach to determine if transmitter co-expression could reliably sub-categorize and explain the apparent heterogeneity of LN cellular properties.

Neuropeptide co-expression is highly heterogeneous

We first determined the pairwise co-expression relationships for GABA and multiple neuropeptides Tachykinin (TK), FMRFamide (FMRF), Allatotropin (Mas-AT), Myoinhibitory peptide (MIP) and Allatostatin-A (AST-A) in LNs (Fig. 1A-E). We chose these neuropeptides because there are available antibodies of sufficient quality, we have performed the proper pre-adsorption controls for each of them, and finally these neuropeptides have the best functional, biochemical, and developmental characterization in *Manduca* as well as other insect species (Carroll et al., 1986; Blackburn et al., 2001; Skaer et al., 2002; Teal, 2002; Utz and Schachtner, 2005; Utz et al., 2007; Yapici et al., 2008; Ignell et al., 2009; Asahina et al., 2014; Ko et al., 2015). All moths were naïve and unmated adults, and equal number of males and females were used for each transmitter combination. Using a paired t-test we found no significant differences between the left and right lateral cell clusters for all peptides: Mas-AT ($t=1.718$; $df=5$; $p=0.1465$), MIP ($t=0.1056$; $df=5$; $p=0.9200$), FMRF ($t=0.5324$;$df=5$; $p=0.6172$), TK ($t=1.085$;$df=5$; $p=0.3276$), AST-A ($t=0.6407$;$df=5$; $p=0.5499$). We also compared counts from male and female moths and using a paired t-test, we found no significant differences in cell counts between males and females for MIP ($t=1.531$; $df=2$;$p= 0.2654$) , AST-A ($t=0.4187$; $df=2$; $p= 0.7161$), TK ($t=0.0000$; $df=2$; $p=1.0$), FMRF ($t=0.1220$; $df=2$; $p=0.9141$). There was a significant difference between males and females in Mas-AT expression ($t=11.97$; $df=2$; $p = 0.0069$). Peptidergic LNs predominantly co-expressed GABA (Fig. 1F, Table 1), suggesting that LNs can be broadly subdivided into

GABAergic/peptidergic and non-GABAergic/non-peptidergic LNs. The non-GABAergic LNs have the potential to be glutamatergic as RT-qPCR on lateral cell cluster mRNA revealed that the vesicular glutamate transporter (vGLUT) was highly expressed relative to a reference gene (40s ribosomal protein s3; RpS3, see Table 3 for Cq values). A large population of glutamatergic LNs in *Manduca*, in addition to the GABAergic LNs, would be consistent with the organization of the *Drosophila* AL (Das et al., 2011; Liu and Wilson, 2013). We then determined the co-expression ratios (i.e. what percentage of X expressing neurons co-express Y) of every pairwise combination of TK, FMRF, Mas-AT and MIP (Fig. 2A-G). There were few consistent co-expression patterns, suggesting that most LNs co-express multiple neuropeptides to a variable degree (Fig. 2 E, G, C). The exception to this rule was TK which was co-expressed 100% with MIP and never co-expressed with FMRF and Mas-AT (Fig. 2A, B, D, H). The 12 TKergic LNs were therefore the only LNs that expressed a consistent transmitter profile. Our results are consistent with other studies of GABA and peptide expression in *Manduca* (Hoskins et al., 1986; Homberg et al., 1990; Utz et al., 2008). Co-expression ratios for each pairwise co-expression relationship (i.e. % of neurons that co-express X and Y) revealed that apart from TK, neuropeptides were co-expressed to a variable degree (Fig. 2H).

Computational analysis of transmitter co-expression reveals that independent expression probability cannot explain observed transmitter co-expression in LNs

Two possible scenarios can explain the lack of apparent systematic association between specific neuropeptides co-expressed by LNs. In one scenario, expression of a given neuropeptide is independent of the expression of another and the likelihood of specific co-expression patterns is equal to the independent probabilities of expression of each transmitter given the number of LNs that express each transmitter. Alternatively, specific pairs of neuropeptides are co-expressed

410 more (or less) often than by chance, and a certain number of such relationships can explain the
411 overall pattern of neuropeptide co-expression. To test these scenarios, we began by using
412 computational modeling to test the hypothesis that co-expression could be explained independent
413 probabilities of expression of each transmitter alone. Given the known total number of LNs in
414 the lateral cell cluster (360;(Homberg et al., 1988) and the total number of LNs expressing each
415 neuropeptide (Fig. 1), the model calculates the probability of a neuron co-expressing two
416 transmitters (Fig. 3A; see methods). The model predicts the percentage of neurons that co-
417 express every pairwise relationship of transmitters in our study. For example, based on the
418 number of LNs that express Mas-AT and the number of LNs that express FMRFamide, and the
419 total number of LNs in the AL, the model determines that 12% of Mas-AT neurons should co-
420 express FMRF if the probability of expressing the former is independent of the probability of
421 expressing the latter. However, based on our immunocytochemical data, we observed that 22%
422 of Mas-AT neurons co-express FMRF (Fig 2H). We then compared every predicted co-
423 expression ratio from the model (which assumes independent probabilities of expression of each
424 transmitter for each pairwise relationship) to the observed co-expression ratios (Fig. 2H) and
425 determined how well the model replicates observed co-expression (Fig. 3B). If co-expression
426 probabilities can be replicated by a model that assumes independent expression of each
427 transmitter, then as a result, no organizing co-expression dependencies will be identified.

428 We found that most co-expression relationships were not replicated by a model assuming
429 independent transmitter expression (Figure 4A; “independent expression” model). To statistically
430 measure how well our model replicated observed co-expression patterns we then used a standard
431 deviation index (SDI) for every predicted pairwise co-expression relationship vs. observed co-
432 expression. An SDI score of 0 indicates that our simulation perfectly recapitulates observed co-

expression patterns, whereas an SDI score above 1 indicates poor performance of the model. Each predicted co-expression ratio from the model was compared to the observed co-expression ratios and a SDI was calculated (SDI = ($Mean_{model}$ – $Mean_{observed}$) /$stdev_{greatest}$). SDI scores for every pairwise co-expression relationship were statistically weighted (see methods), such that co-expression relationships that included a larger proportion of the total LN population carried more weight. SDI scores revealed that while an independent-expression model could replicate some co-expression relationships (with a weighted SDI of 1.49), independent-expression alone does not accurately replicate the observed co-expression (Fig. 4B).

A few specific co-expression constraints allow replication of overall co-expression patterns

Since the independent expression of each transmitter did not replicate the overall probabilities of co-expression patterns, we next sought to identify which co-expression relationship must be adjusted to replicate the overall structure of co-expression. We implemented, in our model, rules according to which the probability of expression of a transmitter is dependent on the expression of another transmitter (Fig 5A), thereby explicitly setting the probability of co-expression to its observed value (Fig 2H). Therefore, the model contains a set number of co-expression relationships in the form of rules (for example, 42% of MIPergic LNs co-express Mas-AT as observed from our immunocytochemistry), while leaving the rest of the relationships to emerge through probabilistically-independent expression. We tested 94 different model iterations, each containing different combinations of 'co-expression rules' to determine which combination(s) of rules best replicated overall observed co-expression (Figure 5B). This allowed us to identify predictive co-expression relationships in an unbiased manner. As expected, the ability of the model to replicate observed co-expression patterns

improved as more rules were added, as shown by weighted SDIs from all model iterations (Fig. 5B-D).

However, some combinations of rules outperformed others. We first constrained the total number of cells in the model to the total number of GABAergic LNs (164 cells instead of 360 total LNs), as presence of GABA is a reliable predictor of peptide expression observed in this study. This constraint outperformed the independent-expression model, had a weighted SDI of 0.94 and accurately replicated more co-expression patterns (Fig. 6A). This suggests that much of the diversity of neuropeptide co-expression can be constrained to the sub-population of GABAergic LNs in our study. All remaining model iterations were constrained to the total number of GABAergic LNs (see Figure 5B, filled in symbols indicate models where total number of LNs = 164 (with stdev) GABAergic neurons). Unexpectedly, one particular model that only contained one co-expression rule outperformed most models that were constrained by 2 and 3 rules (red square Fig. 5B). When the proportion of MIPergic LNs expressing Mas-AT is set to its observed value (42%), the model replicated the highest number of co-expression relationships of all models with one rule (Fig. 6B-D), yielded the lowest weighted SDI (0.36), and outperformed the average of models with one rule (lower 95% CI of mean: 0.6551, upper 95% CI of mean: 0.9862), two rules (lower 95% CI of mean: 0.5450, upper 95% CI of mean: 0.7240), and even 3 rules (lower 95% CI of mean: 0.4736, upper 95% CI of mean: 0.5897). This was surprising because it suggested that replicating observed co-expression patterns did not require all co-expression relationships to be fixed, revealing specific proportional relationships that may be may be predictive of overall observed co-expression patterns.

The only set of co-expression patterns that could not be replicated reasonably well in the model that included the GABA and the MIP/Mas-AT rules (as described above) involves TK.

The 12 TK LNs (Lizbinski et al., 2016) follow a strict all-or-none neuropeptide co-expression pattern (100% co-expression with MIP and 0% co-express with Mas-AT or FMRFamide). Consistent with our data, TK LNs in the AL of the moth, *Heliothis virescens* also do not co-express FMRF or Mas-AT (Berg et al., 2007). This co-expression pattern cannot be replicated through independent expression models, even when several other rules are considered (Fig 6E). These co-expression patterns are so clear-cut that it set TK apart from other transmitters observed in this study.

$GABA_B$ and neuropeptide receptors are expressed across all principal neuron types of the AL

It may be unnecessary to tightly regulate co-expression of neuropeptides in specific sub-populations of LNs simply because specific classes of AL neurons express different sets of neuropeptide receptors. Thus, the heterogeneous transmitter profiles of individual LNs may not matter functionally because the impact of individual peptides within a modulatory cocktail of many peptides may be segregated due to neuron class-specific expression of each receptor. For instance, if olfactory receptor neurons (ORNs) express the MIP receptor and projection neurons (PNs) express the Mas-AT receptor, the influence of these two neuropeptides could differentially target input and output of the network, rather target the same neuron, resulting in different consequences on the network. However, this does not appear to be the case in this network, as we did not find differential expression of the receptors for the peptides examined in this study between ORNs, LNs and PNs. We first identified transcripts from the *Manduca* genome (Kanost et al., 2016) with high sequence identity to neuropeptide receptors identified from reference genomes in closely related species (Table 2). Then, using RT-qPCR, we determined the relative expression of five neuropeptide receptors (Mas-AT, MIP, AST-A, FMRF, TK), and the $GABA_B$

receptor in mRNA from the antennae (which house ORNs), the medial cell cluster (which houses only PNs), the lateral cell cluster (which houses LNs and PNs) and whole brains (as a positive control). Although the receptors for Mas-AT, MIP, AST-A, FMRF, $GABA_B$, were detected in all four tissue types, the TK receptor was not detected in the lateral cell cluster (Fig. 7, for raw qPCR data see Table 3). This suggests that TKergic LNs differ from other LNs both in their co-expression patterns and their postsynaptic targets. Although we could not assess receptor expression on a neuron-by-neuron basis, our results suggest that a single LN releasing neuropeptides from at least four individual peptide families can have a powerful effect on the network, potentially affecting all three major cell classes in the AL.

***Discussion*:**

Broad neuronal classes are surprisingly heterogeneous across many parameters and sub-classes often exhibit partially overlapping traits including transmitter co-expression. Our goal was to determine organizing principles of LN heterogeneity. Our results suggest that neuropeptide co-expression in the AL is both heterogeneous and partially overlapping across the entire population rather than consistent within specific sub-populations of LNs (Fig. 8). Thus, peptidergic modulation cannot be considered within the context of *single* neuropeptides as activation of any given LN results in a dynamic cocktail of modulators that have the potential to influence every level of olfactory processing within the AL. Specifically, we find that transmitter profile is heterogeneous across LNs, with individual olfactory LNs capable of expressing the main inhibitory transmitter GABA and peptides from at least four families, and few instances in which transmitters are consistently co-expressed. Observed co-expression patterns cannot be explained by independent probabilities of expression of each transmitter (Fig. 4). Our analyses point to three organizing principles that once taken into consideration allow replication of overall

co-expression structure: 1- peptidergic neurons are highly likely to co-express GABA; 2- the probability of expressing Mas-AT is dependent on MIP expression; 3- the all-or-none co-expression patterns of TKergic neurons with several other neuropeptides (MIP, FMRF and Mas-AT). For other pairs, the presence of one transmitter was not predictive of the presence of the other and thus co-expression probability could be replicated by independent probabilities. The stochastic nature of these co-expression patterns argues against clear-cut, exclusive definition of subpopulations based on the presence of single neuropeptides. Furthermore, the receptors for GABA and all neuropeptides in this study were expressed within each population of principal neuron type in the AL (Fig. 7) suggesting that peptides released from LNs potentially influence every level of olfactory processing within the AL. Overall, we demonstrate that peptide expression is partially overlapping across LNs and thus sub-populations of LNs cannot be functionally defined based on the presence of single peptides. Furthermore, neuropeptide and $GABA_B$ receptors were expressed within each population of principal neuron type in the AL because ORNs, the influence of peptides are not segregated based on cell class-specific receptor expression. Thus, co-release of peptides and GABA likely mediate a complex mix modulation to control the dynamic range of the AL, providing multiple mechanisms to alter olfactory processing.

Heterogeneous transmitter co-expression is a common theme within GABAergic LNs across vertebrates and invertebrates alike (Homberg et al., 1990; Maccaferri and Lacaille, 2003; Flames and Marin, 2005; Utz et al., 2008; Carlsson et al., 2010; DeFelipe et al., 2013; Siju et al., 2013; Binzer et al., 2014; Gabitto et al., 2016; Yavorska and Wehr, 2016; Diesner et al., 2018b). MALDI-TOF spectrometry revealed that at least 12 known peptides are expressed in developing *Manduca* ALs (Utz et al., 2007), suggesting that co-expression patterns are likely even more

complex than detailed here. Furthermore, the antibodies used in this study recognize multiple isoforms of peptides within the same family (i.e. FMRF has multiple isoforms), and thus there are almost certainly more organizational principals underlying heterogeneous peptide expression than discussed here. Other insects including mosquitos (Siju et al., 2013), other species of moths (Berg et al., 2007; Diesner et al., 2018b), beetles (Binzer et al., 2014) and fruit flies (Carlsson et al., 2010; Hussain et al., 2016; Croset et al., 2018), express a large number of peptides within their olfactory systems suggesting that peptides likely play an important yet functionally underexplored role in shaping olfactory responses. One exception to the theme of heterogeneous co-expression was that the TK neurons differed in their patterns of co-expression from other peptidergic LNs. All TK LNs co-expressed MIP, and none co-expressed FMRF or Mas-AT, suggesting that TK LNs are primarily inhibitory as TK and MIP receptors are inhibitory in *Drosophila* (Yapici et al., 2008; Ignell et al., 2009; Ko et al., 2015). Furthermore, TK receptor transcripts were not detected in lateral cell cluster mRNA and thus not in LNs, although TK/MIPergic LNs could still influence LNs via $GABA_B$ and MIP receptor. In *Drosophila melanogaster*, TK mediates presynaptic gain control upon ORNs (Ignell et al., 2009), and TKr expression in *Manduca* ORNs is consistent with this finding. This suggests that TK LNs may play a distinct role from other LNs in olfactory processing which could include presynaptic gain control.

Very few non-GABAergic LNs co-express the neuropeptides we examined here, however they are still a sizeable proportion of the total number of LNs and likely as heterogeneous as GABAergic LNs. We did not definitively identify the transmitter released by these LNs, however we did detect the expression of vGlut mRNA within the lateral cell cluster (Fig. 7), making glutamate a candidate transmitter for the non-GABAergic LNs. Similar to GABAergic

570 LNs, glutamatergic LNs in *Drosophila* are particularly diverse in their morphology (Das et al.,
571 2011) but appear to differ from GABAergic LNs in their synaptic targets by predominantly
572 affecting PNs (Liu and Wilson, 2013), while GABAergic LNs in *Drosophila* affect ORNs, LNs
573 and PNs (Wilson and Laurent, 2005; Olsen and Wilson, 2008; Root et al., 2008; Hong and
574 Wilson, 2015). Future studies should confirm whether the non-GABAergic population observed
575 here are truly glutamatergic.

576 The probability of expression of certain transmitters appear to be dependent on one
577 another. In particular, we showed that the probability of expressing Mas-AT is dependent on the
578 expression of MIP (Figure 6). While the goal of our study is not to determine the developmental
579 mechanisms that underlie co-expression, it is important to note that developmental mechanisms
580 of peptidergic regulation most certainly shape observed heterogeneous co-expression. For
581 instance, the molting hormone 20-hydroxyecdysone induces Mas-AT expression in LNs and
582 other neuropeptides in the AL of *Manduca* (Utz and Schachtner, 2005; Utz et al., 2007),
583 implying that co-expression patterns may reflect extrinsic developmental cues that guide the
584 development of specific peptide expressing LNs. Furthermore, both Mas-AT and MIP expressing
585 LNs arise slightly before and during the formation of glomeruli, suggesting that temporal
586 expression patterns of these peptides may play a role in the development of AL structure and
587 function (Utz et al., 2007). Interestingly, the model constraint best able to replicate observed co-
588 expression across all LNs in our study was the proportional relationship between MIP/Mas-AT
589 expressing neurons.

590 However, the developmental mechanisms that control peptide expression in LNs of
591 *Manduca* are unknown. In *Drosophila*, the transcription factor DIMMED targets many genes
592 involved in peptide expression (Hewes et al., 2003; Gauthier and Hewes, 2006; Hewes et al.,

2006; Park et al., 2008b; Park and Taghert, 2009; Hadzic et al., 2015) and dense core vesicle production (Hamanaka et al., 2010; Park et al., 2014). DIMMED likely acts in a combinatorial manner with other cell-specific transcription factors to determine peptide expression in individual neurons (Liu et al., 2016; Stratmann and Thor, 2017). Although DIMMED doesn't target any single neuropeptide gene (Hadzic et al., 2015) other transcription factors do regulate sub-type specific neuropeptide expression (Allan et al., 2003; Berndt et al., 2015). While DIMMED positive neurons co-express multiple peptides, not all peptidergic neurons express DIMMED (Park et al., 2008a; Diesner et al., 2018a), and the role DIMMED of in *Manduca* has not been established. Regardless, a similar combinatorial transcriptional code could underlie the heterogeneity of peptide expression observed here. Furthermore, in cortex, LN subtypes arise from unique progenitors (Anderson et al., 1997; Wichterle et al., 2001; Nery et al., 2002; Kepecs and Fishell, 2014) and their diversity is shaped by additional factors (Flames and Marin, 2005) including neural activity (Patz et al., 2004; De Marco Garcia et al., 2011) transcription factor expression (Mayer et al., 2018; Sweeney et al., 2018) and growth factors (Huang et al., 1999). Similarly, GABAergic and glutamatergic LNs in *Drosophila* arise from distinct neuroblasts (Das et al., 2008; Das et al., 2011), and glomerular innervation patterns of LNs require ORN axons during development (Chou et al., 2010), suggesting that heterogeneity of LNs may be due in part to distinct origins and/or activity of other neurons in the network.

Our study reveals some expression co-dependencies, but also highlights the apparent stochastic nature of other co-expression patterns. There are several examples of biological systems in which features like gene expression in *E. coli* clones (Elowitz et al., 2002; Raj and van Oudenaarden, 2008; Huh and Paulsson, 2011), behavior (Honegger and de Bivort, 2018), or anatomical layout (Caron et al., 2013), appear to be randomly structured or stochastic. For

example, random combinations of AL PNs from different glomeruli converge and synapse upon individual mushroom body Kenyon cells in *Drosophila* regardless of anatomy, developmental origin or odor tuning, thus abandoning the odor-topic organization of the AL (Caron et al., 2013). Due to the stochastic heterogeneity of some transmitter co-expression patterns, our results suggest the presence of single peptides should not be used to functionally define classes of neurons. Additionally, this stochasticity suggests that LNs may not functionally require fixed compliments of transmitters.

We found that a single neuropeptide has the potential to simultaneously target every principal neuron type as all neuropeptide receptors were expressed by populations of ORNs, LNs and PNs. This network wide convergence of peptidergic modulation demonstrates that individual LNs do not differentially target principal neuron type based on differences in post-synaptic receptor expression. This further supports the idea that LN activation may serve to regulate multiple processing stages within the olfactory network by simultaneously targeting AL input, output and local processing. However, individual neurons within each principal AL neuron type may exhibit differential receptor expression, as we were not able to assess receptor expression at the level of individual neurons. Future studies should determine if neuropeptide receptor expression is as heterogeneous as neuropeptide co-expression itself as there are likely sub-populations of neurons that exhibit differential receptor expression. This may be further complicated as neuropeptide receptor expression can be regulated by physiological state, as observed for the role of hunger (Ko et al., 2015; Min et al., 2016) or mating state in *Drosophila* (Hussain et al., 2016). Peptide expression itself may be similarly regulated, as observed in feeding state of *Aedes aegypti* (Christ et al., 2017) or mating state of *Agrotis ipsilon* moths

638 (Diesner et al., 2018b). All moths in our study were naïve and unmated, however this does not
639 rule out the potential for physiological state to affect peptide expression in the AL.

640 Activation of even a single LN can mediate a complex mix of inhibition and/or
641 excitation that varies in time course and strength due to the co-release of the small-transmitter
642 GABA and a heterogeneous mix of peptides. LNs, apart from TK LNs, co-expressed multiple
643 peptide families and GABA that activate both inhibitory (TK, sNPF, and sex-peptide/MIP)
644 (Yapici et al., 2008; Ignell et al., 2009; Asahina et al., 2014; Ko et al., 2015) and excitatory
645 receptors (Mas-AT and FMRF) (Horodyski et al., 2011; Lenz et al., 2015; Ormerod et al., 2015)
646 via a mix of ionotropic and metabotropic signaling. Furthermore, AL neurons express both the
647 GABAa and $GABA_B$ receptors, and the effects $GABA_B$ receptor activation are far shorter-lasting
648 relative to neuropeptide receptors (Salio et al., 2006). Thus, small-transmitter and peptide co-
649 expression expands the temporal scale with which a single neuron can alter network processing.
650 However, it is unclear whether LNs employ bulk and/or restricted synaptic release of peptides,
651 making the spatial scale of their influence unknown. Finally, the network may need to be more
652 strongly activated (i.e. by higher concentrations of odors or increased length of odor-stimuli) for
653 LNs to release neuropeptides due to the different calcium binding affinities of distinct
654 synaptotagmins associated with small clear vesicles and dense-core vesicles (Saraswati et al.,
655 2007; Li et al., 2009). Thus, the consequences of LN activation and peptidergic modulation may
656 depend more upon the degree of network activity rather than the identity of any singular LN that
657 is activated. Overall, this heterogeneous cocktail of peptides likely provides the AL with flexible
658 options to up or down regulate olfactory processing over a variety of time frames and spatial
659 scales within the context of ongoing network activity.

Within the AL, combined GABAergic and peptide release from LNs could potentially play a variety of functional roles including autoinhibition, lateral excitation or inhibition, disinhibition, and even odor-specific processing. For example, lateral input from LNs scales with overall network activity as a means to control the dynamic range of the network and avoid response saturation of PNs (Olsen and Wilson, 2008; Root et al., 2008). Additionally, some glomeruli are more subject to inhibition than others simply due to differences in glomerulus-specific, non-uniform LN innervation (Wilson and Laurent, 2005; Chou et al., 2010) and ORN GABAb receptor expression (Root et al., 2008). As a result, the processing of specific odors differs in the degree of insulation from ongoing activity in the olfactory system, and specific glomeruli are therefore more (or less) insulated from presynaptic gain control mediated by both GABA (Root et al., 2008) and, potentially, neuropeptides (Ignell et al., 2009; Ko et al., 2015; Hussain et al., 2016). Spatial activation of *Drosophila* LNs is also odor-specific and heterogeneous, with LNs responding to either single, or multiple odors (Ng et al., 2002). The non-uniform innervation and heterogeneous odor-evoked responses of LNs suggests that the activation of LNs is a complex combinatorial process resulting in glomerular specific local processing. In *Manduca*, most GABAergic LNs are wide-field and heavily ramify all glomeruli, suggesting that the consequences of GABAergic LN activation cannot be fully segregated based on odor identity. However, a small sub-set of GABAergic and non-GABAergic LNs exhibit restricted glomerular arborizations, only innervating a small sub-section of the AL (Reisenman et al., 2011). Consequently, activation of morphologically restricted LNs may dis-inhibit or inhibit other LNs from neighboring glomeruli in an odor-specific manner in order to increase or decrease odor salience by altering the output of PNs (Hildebrand et al., 1992; Christensen et al., 1993). While no correlations between morphology (wide-field vs. restricted), physiology, odor-

683 response profile, and transmitter content have been identified in *Manduca* LNs (Reisenman et al.,
684 2011), it could be that wide-field vs. restricted LNs exhibit distinct and predictable combinations
685 of peptides. These potential network consequences are likely applicable across insect species as
686 LN heterogeneity is a recurring theme. Using physiology paired with hierarchical clustering
687 based on morphology, multiple *Drosophila* LN subtypes exhibit broad correlations between
688 morphology, physiology and genetic classes (Chou et al., 2010). However, LNs within the
689 "patchy" cell type exhibit highly variable innervation patterns and considerable diversity exists
690 even within other LN sub-types (Chou et al., 2010). Additionally, morphologically and
691 functionally distinct classes of LNs exist in honeybees (Schafer and Bicker, 1986; Flanagan and
692 Mercer, 1989; Fonta et al., 1993; Sun et al., 1993; Bornhauser and Meyer, 1997; Seidel and
693 Bicker, 1997; Galizia and Kimmerle, 2004; Dacks et al., 2010) and cockroaches (Malun, 1991;
694 Distler and Boeckh, 1997; Loesel and Homberg, 1999; Husch et al., 2009a, b; Fusca et al., 2013;
695 Fusca et al., 2015; Neupert et al., 2018). Ultimately, determining the roles of individual peptides
696 will be challenging as complex patterns of co-expression must be integrated with knowledge of
697 functionally distinct subtypes of LNs.

698 Reconciling within cell-type heterogeneity represents an ongoing challenge. Similar to
699 LNs across taxa and brain region, *Manduca* LNs are highly heterogeneous across many
700 parameters. This heterogeneity provides multiple coding strategies and mechanisms to neurons
701 within the same population, expanding the role single neurons play in altering network function.
702 The link between heterogeneous response properties and neural coding has been studied in a
703 wide range of systems (Chelaru and Dragoi, 2008; Marsat and Maler, 2010; Ogawa et al., 2011;
704 Pitkow and Meister, 2012; Ahn et al., 2014), however, the systematic analysis of heterogeneous
705 traits like transmitter co-expression has not been as extensively explored. Here, we show that

traits, like transmitter co-expression are partially overlapping across the entire LN population. Ultimately, our results demonstrate that peptidergic modulation cannot be considered within the context of *single* neuropeptides as activation of any given LN results in a dynamic cocktail of modulators that have the potential to influence every level of olfactory processing within the AL.

Author Contributions: All authors had full access to all the data in the study and take responsibility for the integrity of the data and the accuracy of the data analysis. Study concept and design: Kristyn M. Lizbinski (KML), Gary Marsat (GM), Andrew M. Dacks (AMD). Acquisition of data: KML Computational model: KML, GM. Analysis and interpretation of data: KML, GM, AMD. Drafting of the manuscript: KML, GM, AMD. Critical revision of the manuscript for important intellectual content: KML, GM, AMD. Obtained funding: AMD Administrative, technical, and material support: AMD. Study supervision: AMD

Figure Legends:

Figure 1: Peptidergic LNs predominantly co-express GABA. Dashed lines = co-expressed. Solid lines = not co-expressed. **A:** Lateral cell cluster (LCC) labeled for GABA (magenta) and Tachykinin (TK; white). **B:** LCC labeled for GABA (magenta) and Allatotropin (Mas-AT; yellow). **C:** LCC labeled for GABA (magenta) and Myoinhibitory peptide (MIP; orange). **D:** LCC labeled for GABA (magenta) and FMRFamide (cyan). **E:** LCC labeled for GABA (magenta) and Allatostatin-A (AST-A; green). **F:** Bar graph of average number of cell bodies (above bars) that express each transmitter type per AL and the percentage (within bars) of each neuropeptide population per AL that co-express GABA. See Table 2 for averages and standard deviations. n = 6 animals per combination. All scale bars = 50um.

Figure 2: Neuropeptide co-expression is heterogeneous. Dashed lines = co-expressed. Solid lines= not co-expressed. Co-expression for **A,B:** TK (white) and Mas-AT (yellow), **C:** FMRFamide (cyan) and Mas-AT, **D:** TK and MIP (orange), **E:** Mas-AT and MIP, **F:** FMRFamide and MIP and **G:** TK and FMRFamide. All scale bars = 50um. **H:** Schematic representation of transmitter co-expression by LNs. Each circle represents the population of LNs that express a given transmitter. Arrow width and percentage located at arrowhead represent proportion of a given LN type (arrow origin) that also express a second transmitter (arrow destination). FMRFamide and MIP co-expression could not be calculated for technical reasons (see methods). No TK LNs co-expressed FMRFamide or Mas-AT. Non-GABAergic LNs are not depicted.

Figure 3: Schematic representations of the computational model used to calculate the probability of LN co-expression patterns A: Each column represents a transmitter, the number of rows corresponds to the total # of neurons in the population (reduced in this illustration to 5 total cells for the sake of simplicity, 360 LNs in reality). The number of neurons in each column that are transmitter positive correspond to the average number of neurons (standard deviations built in) that express each transmitter that we observed using immunocytochemistry (see Figure 1F and Table 1 for values). The model then sums across each row in a pairwise fashion to determine the co-expression percentage of a given transmitter pair. For example, for TK/MIP, the model would predict that 1/3 or 33% of MIP neurons (orange) would co-express TK assuming independent probabilities of expression for each transmitter. **B:** Schematic representation comparing predicted co-expression percentages from the "independent expression" model to our observed co-expression patterns. Each circle represents a population of LNs that express a given transmitter. Given the number of neurons that express each individual transmitter (values in Fig. 1F and Table 1), the model calculates the probability that a neuron will co-express two transmitters. Line thickness represents degree to which transmitters are co-expressed. We then compare the predicted co-expression from our "independent expression" model to our observed co-expression values to see if observed co-expression can be explained based on independent probability of expression.

Figure 4: Computational analysis of transmitter co-expression reveals that independent expression probability cannot explain observed transmitter co-expression in LNs A: Predicted co-expression percentages for every pairwise relationship from the independent co-expression model (red) vs. observed co-expression percentages (black). A model that assumes independent probability of co-expression could not replicate observed co-expression percentages. **B:** Statistical comparison of the independent co-expression model's prediction vs. observed co-expression reveals that independent probability of co-expression alone cannot replicate observed LN co-expression patterns. Each colored rectangle represents an individual pair-wise relationship (e.g TK/Mas-AT). Standard deviation indices (SDI) were calculated for every pairwise relationship to determine how closely the model could replicate observed co-expression. An SDI of 0 (blue) denotes no statistical difference between observed co-expression and predicted co-expression from the model, thus representing co-expression relationships that the model was able to replicate very well. SDI values above 1 indicate a poor match between the model and observed values.

Figure 5: A few specific co-expression constraints allow replication of overall co-expression patterns A: Model constraints are applied to explicitly set the probability of a co-expression relationship to its observed value. In this example, a constraint is set in which 100% of TK LNs co-express MIP, while leaving the remaining relationships to emerge through probabilistically independent expression. This model is then compared to observed co-expression data. **B**: Specific rules outperform others at replicating observed co-expression patterns. Open circle represents model run with total number of LNs set to 360. Closed symbols represent models runs with total number of neurons set to the total number of GABAergic LNs (180). Red denotes

standout iterations of the model that best replicated observed co-expression. The single rule that shifted the prediction closest to observed co-expression was when the proportional relationship between MIP/Mas-AT was set as a static rule in the model (red square). The two rules that shifted the prediction closest to observed co-expression were MIP/Mas-AT and TK/Mas-AT. The three rules that shifted the prediction closest to observed co-expression were TK/Mas-AT + Mas-AT/MIP + FMRF/Mas-AT. **C**: Weighted SDI values for various model iterations. The model improves as more rules are added. **D**: Percent improvement of each model's predictive power with respect to the independent expression model. Both GABA constraint and MIP/Mas-AT rule drastically improved the model's ability to replicate co-expression patterns. Note that the MIP/Mas-AT rule model even outperformed the average prediction of all models containing three rules.

Figure 6: MIP/Mas-AT co-expression rule best biases the model to replicate observed co-expression patterns A: Reducing the total number of neurons in the model to the total number of GABAergic LNs (180), improves model performance. SDI = 0 (blue) denotes no statistical difference between observed co-expression and predicted co-expression. SDI > 1 indicates a poor match between the model and observed values. **B:** Constraining the model based on MIP/Mas-AT co-expression causes the model to reliably replicate many observed co-expression patterns. A model following this single rule outperformed the average of all models containing three set co-expression rules. **C:** All predicted pairwise co-expression percentages from the model following the MIP/Mas-AT rule (blue) vs. observed co-expression percentages (black). **D:** Neither independent (red), nor ind_GABA (grey) models reliably replicated observed co-expression patterns (Mas-AT/FMRF used as an example). However, the MIP/Mas-AT (blue) constraint best replicates observed co-expression patterns (denoted by black arrow). **E:** Observed TK co-expression patterns (TK/Mas-AT used an example) were not reliably replicated by any model iteration; independent expression model prediction (red), ind_GABA model (grey), and MIP/Mas-AT model prediction (blue).

Figure 7: Neuropeptide and $GABA_B$ receptor expression across principal neuron types of the AL. Relative receptor expression for Mas-ATr, MIPr, ASTr, FMRFr, $GABA_Br$ are present in all tissue types and therefore expressed in ORNs, LNs and PNs in varying expression levels. Cartoons on the x-axis represent the tissue type (blue) used to extract mRNA from each population of principal olfactory cell types. TK was not detectable (N.D.) in lateral cell cluster mRNA and therefore not detectable in LNs. RpS3 was used as the reference gene. See Table 2 for primer sequences and Table 3 for raw Cq values for all receptors.

Figure 8: Heterogeneous transmitter co-expression in LNs blurs sub-divisions. While LNs can be broadly subdivided based on small transmitter (GABA vs. non-GABAergic (glutamatergic?)), co-expression within the GABAergic class reveals that LNs sub-classes cannot be identified on individual transmitter expression alone. Neuropeptide co-expression in the AL is both heterogeneous and partially overlapping across the entire population rather than consistent within specific sub-populations of LNs.

Extended Data 1:
These MatLab scripts calculate the probability of a given neuron co-expressing two neurotransmitters. The script calculates co-expression probabilities for a population of 360 neurons that individually express GABA, Myoinhibitory peptide (MIP), Tachykinin (TK), FMRFamide. Code can be altered to include the total # of neurons in a given neural population and the avg # (and stdev) of neurons that express each transmitter. The probability_script assumes no expression dependencies, and thus the predicitons of co-expression are based purely on independent expression probability.

Extended Data 2:
Similarly, the script_Predict_FMRF_Mas-AT script allows you to explicity set the co-expression probability of two given transmitters to its observed value. For example, you may know that 30% of FMRF expressing neurons also express the transmitter Mas-AT based on physical data from immunocytochemistry. This relationship is then set as an explicit rule and co-expression dependency, leaving the remaining co-expression relationships to emerge based on independent probablility of expression. This allowed us to determine if there are dependent co-expression relationships in your population of neurons that may be predictive of other relationships in the population in an unbiased manner.

Works Cited

Ache BW, Young JM (2005) Olfaction: diverse species, conserved principles. Neuron 48:417-430.

Ahn J, Kreeger LJ, Lubejko ST, Butts DA, MacLeod KM (2014) Heterogeneity of intrinsic biophysical properties among cochlear nucleus neurons improves the population coding of temporal information. Journal of neurophysiology 111:2320-2331.

Allan DW, St Pierre SE, Miguel-Aliaga I, Thor S (2003) Specification of neuropeptide cell identity by the integration of retrograde BMP signaling and a combinatorial transcription factor code. Cell 113:73-86.

Anderson SA, Eisenstat DD, Shi L, Rubenstein JL (1997) Interneuron migration from basal forebrain to neocortex: dependence on Dlx genes. Science 278:474-476.

Asahina K, Watanabe K, Duistermars BJ, Hoopfer E, Gonzalez CR, Eyjolfsdottir EA, Perona P, Anderson DJ (2014) Tachykinin-expressing neurons control male-specific aggressive arousal in Drosophila. Cell 156:221-235.

Bell RA, Joachim FG (1976) Techniques for Rearing Laboratory Colonies of Tobacco Hornworms and Pink Bollworms Lepidoptera-Sphingidae-Gelechiidae. Annals of the Entomological Society of America 69:365-373.

Berg BG, Schachtner J, Utz S, Homberg U (2007) Distribution of neuropeptides in the primary olfactory center of the heliothine moth Heliothis virescens. Cell Tissue Res 327:385-398.

Berndt AJ, Tang JC, Ridyard MS, Lian T, Keatings K, Allan DW (2015) Gene Regulatory Mechanisms Underlying the Spatial and Temporal Regulation of Target-Dependent Gene Expression in Drosophila Neurons. PLoS genetics 11:e1005754.

Binzer M, Heuer CM, Kollmann M, Kahnt J, Hauser F, Grimmelikhuijzen CJ, Schachtner J (2014) Neuropeptidome of Tribolium castaneum antennal lobes and mushroom bodies. The Journal of comparative neurology 522:337-357.

869 Blackburn MB, Jaffe H, Kochansky J, Raina AK (2001) Identification of four additional myoinhibitory
870 peptides (MIPs) from the ventral nerve cord of Manduca sexta. Archives of insect biochemistry
871 and physiology 48:121-128.
872 Bornhauser BC, Meyer EP (1997) Histamine-like immunoreactivity in the visual system and brain of an
873 orthopteran and a hymenopteran insect. Cell Tissue Res 287:211-221.
874 Bradley SP, Chapman PD, Lizbinski KM, Daly KC, Dacks AM (2016) A Flight Sensory-Motor to Olfactory
875 Processing Circuit in the Moth Manduca sexta. Frontiers in neural circuits 10:5.
876 Carlsson MA, Diesner M, Schachtner J, Nässel DR (2010) Multiple neuropeptides in the Drosophila
877 antennal lobe suggest complex modulatory circuits. The Journal of comparative neurology
878 518:3359-3380.
879 Caron SJ, Ruta V, Abbott LF, Axel R (2013) Random convergence of olfactory inputs in the Drosophila
880 mushroom body. Nature 497:113-117.
881 Carroll LS, Carrow GM, Calabrese RL (1986) Localization and release of FMRFamide-like
882 immunoreactivity in the cerebral neuroendocrine system of Manduca sexta. The Journal of
883 experimental biology 126:1-14.
884 Chelaru MI, Dragoi V (2008) Efficient coding in heterogeneous neuronal populations. Proceedings of the
885 National Academy of Sciences of the United States of America 105:16344-16349.
886 Chou YH, Spletter ML, Yaksi E, Leong JC, Wilson RI, Luo L (2010) Diversity and wiring variability of
887 olfactory local interneurons in the Drosophila antennal lobe. Nature neuroscience 13:439-449.
888 Christ P, Reifenrath A, Kahnt J, Hauser F, Hill SR, Schachtner J, Ignell R (2017) Feeding-induced changes in
889 allatostatin-A and short neuropeptide F in the antennal lobes affect odor-mediated host seeking
890 in the yellow fever mosquito, Aedes aegypti. PloS one 12:e0188243.
891 Christensen TA, Hildebrand JG (1987) Male-specific, sex pheromone-selective projection neurons in the
892 antennal lobes of the moth Manduca sexta. J Comp Physiol A 160:553-569.
893 Christensen TA, Waldrop BR, Harrow ID, Hildebrand JG (1993) Local interneurons and information
894 processing in the olfactory glomeruli of the moth Manduca sexta. J Comp Physiol A 173:385-399.
895 Cohen JY, Amoroso MW, Uchida N (2015) Serotonergic neurons signal reward and punishment on
896 multiple timescales. eLife 4.
897 Croset V, Treiber CD, Waddell S (2018) Cellular diversity in the Drosophila midbrain revealed by single-
898 cell transcriptomics. eLife 7.
899 Dacks AM, Reisenman CE, Paulk AC, Nighorn AJ (2010) Histamine-immunoreactive local neurons in the
900 antennal lobes of the hymenoptera. The Journal of comparative neurology 518:2917-2933.
901 Daly KC, Kalwar F, Hatfield M, Staudacher E, Bradley SP (2013) Odor detection in Manduca sexta is
902 optimized when odor stimuli are pulsed at a frequency matching the wing beat during flight.
903 PloS one 8:e81863.
904 Das A, Sen S, Lichtneckert R, Okada R, Ito K, Rodrigues V, Reichert H (2008) Drosophila olfactory local
905 interneurons and projection neurons derive from a common neuroblast lineage specified by the
906 empty spiracles gene. Neural Dev 3:33.
907 Das A, Chiang A, Davla S, Priya R, Reichert H, Vijayraghavan K, Rodrigues V (2011) Identification and
908 analysis of a glutamatergic local interneuron lineage in the adult Drosophila olfactory system.
909 Neural Syst Circuits 1:4.
910 De Marco Garcia NV, Karayannis T, Fishell G (2011) Neuronal activity is required for the development of
911 specific cortical interneuron subtypes. Nature 472:351-355.
912 DeFelipe J et al. (2013) New insights into the classification and nomenclature of cortical GABAergic
913 interneurons. Nature reviews Neuroscience 14:202-216.
914 Diesner M, Predel R, Neupert S (2018a) Neuropeptide Mapping of Dimmed Cells of Adult Drosophila
915 Brain. Journal of the American Society for Mass Spectrometry.

916 Diesner M, Gallot A, Binz H, Gaertner C, Vitecek S, Kahnt J, Schachtner J, Jacquin-Joly E, Gadenne C
917 (2018b) Mating-Induced Differential Peptidomics of Neuropeptides and Protein Hormones in
918 Agrotis ipsilon Moths. Journal of proteome research.
919 Distler PG, Boeckh J (1997) Synaptic connections between identified neuron types in the antennal lobe
920 glomeruli of the cockroach, Periplaneta americana: II. Local multiglomerular interneurons. The
921 Journal of comparative neurology 383:529-540.
922 Eddine R, Valverde S, Tolu S, Dautan D, Hay A, Morel C, Cui Y, Lambolez B, Venance L, Marti F, Faure P
923 (2015) A concurrent excitation and inhibition of dopaminergic subpopulations in response to
924 nicotine. Scientific reports 5:8184.
925 Elowitz MB, Levine AJ, Siggia ED, Swain PS (2002) Stochastic gene expression in a single cell. Science
926 297:1183-1186.
927 Flames N, Marin O (2005) Developmental mechanisms underlying the generation of cortical interneuron
928 diversity. Neuron 46:377-381.
929 Flanagan D, Mercer A (1989) Morphology and response characteristics of neurones in the
930 deutocerebrum of the brain in the honeybeeApis mellifera. Journal of comparative physiology A,
931 Neuroethology, sensory, neural, and behavioral physiology 164:483-494.
932 Fonta C, Sun X, Masson C (1993) Morphology and spatial distribution of bee antennal lobe interneurones
933 responsive to odours. Chemical senses 18:101-119.
934 Fusca D, Schachtner J, Kloppenburg P (2015) Colocalization of allatotropin and tachykinin-related
935 peptides with classical transmitters in physiologically distinct subtypes of olfactory local
936 interneurons in the cockroach (Periplaneta americana). The Journal of comparative neurology
937 523:1569-1586.
938 Fusca D, Husch A, Baumann A, Kloppenburg P (2013) Choline acetyltransferase-like immunoreactivity in
939 a physiologically distinct subtype of olfactory nonspiking local interneurons in the cockroach
940 (periplaneta americana). The Journal of comparative neurology 521:3556-3569.
941 Gabitto MI, Pakman A, Bikoff JB, Abbott LF, Jessell TM, Paninski L (2016) Bayesian Sparse Regression
942 Analysis Documents the Diversity of Spinal Inhibitory Interneurons. Cell 165:220-233.
943 Galizia CG, Kimmerle B (2004) Physiological and morphological characterization of honeybee olfactory
944 neurons combining electrophysiology, calcium imaging and confocal microscopy. Journal of
945 comparative physiology A, Neuroethology, sensory, neural, and behavioral physiology 190:21-
946 38.
947 Gauthier SA, Hewes RS (2006) Transcriptional regulation of neuropeptide and peptide hormone
948 expression by the Drosophila dimmed and cryptocephal genes. The Journal of experimental
949 biology 209:1803-1815.
950 Gonchar Y, Wang Q, Burkhalter A (2007) Multiple distinct subtypes of GABAergic neurons in mouse
951 visual cortex identified by triple immunostaining. Frontiers in neuroanatomy 1:3.
952 Hadzic T, Park D, Abruzzi KC, Yang L, Trigg JS, Rohs R, Rosbash M, Taghert PH (2015) Genome-wide
953 features of neuroendocrine regulation in Drosophila by the basic helix-loop-helix transcription
954 factor DIMMED. Nucleic acids research 43:2199-2215.
955 Hamanaka Y, Park D, Yin P, Annangudi SP, Edwards TN, Sweedler J, Meinertzhagen IA, Taghert PH (2010)
956 Transcriptional orchestration of the regulated secretory pathway in neurons by the bHLH
957 protein DIMM. Current biology : CB 20:9-18.
958 Hewes RS, Park D, Gauthier SA, Schaefer AM, Taghert PH (2003) The bHLH protein Dimmed controls
959 neuroendocrine cell differentiation in Drosophila. Development 130:1771-1781.
960 Hewes RS, Gu T, Brewster JA, Qu C, Zhao T (2006) Regulation of secretory protein expression in mature
961 cells by DIMM, a basic helix-loop-helix neuroendocrine differentiation factor. The Journal of
962 neuroscience : the official journal of the Society for Neuroscience 26:7860-7869.

963 Hildebrand JG, Christensen TA, Harrow ID, Homberg U, Matsumoto SG, Waldrop BR (1992) The roles of
964 local interneurons in the processing of olfactory information in the antennal lobes of the moth
965 Manduca sexta. Acta Biol Hung 43:167-174.
966 Homberg U, Montague RA, Hildebrand JG (1988) Anatomy of antenno-cerebral pathways in the brain of
967 the sphinx moth Manduca sexta. Cell Tissue Res 254:255-281.
968 Homberg U, Kingan TG, Hildebrand JG (1990) Distribution of FMRFamide-like immunoreactivity in the
969 brain and suboesophageal ganglion of the sphinx moth Manduca sexta and colocalization with
970 SCPB-, BPP-, and GABA-like immunoreactivity. Cell Tissue Res 259:401-419.
971 Honegger K, de Bivort B (2018) Stochasticity, individuality and behavior. Current biology : CB 28:R8-R12.
972 Hong EJ, Wilson RI (2015) Simultaneous encoding of odors by channels with diverse sensitivity to
973 inhibition. Neuron 85:573-589.
974 Horodyski FM, Verlinden H, Filkin N, Vandersmissen HP, Fleury C, Reynolds SE, Kai ZP, Broeck JV (2011)
975 Isolation and functional characterization of an allatotropin receptor from Manduca sexta. Insect
976 Biochem Mol Biol 41:804-814.
977 Hoskins SG, Homberg U, Kingan TG, Christensen TA, Hildebrand JG (1986) Immunocytochemistry of
978 GABA in the antennal lobes of the sphinx moth Manduca sexta. Cell Tissue Res 244:243-252.
979 Huang ZJ, Kirkwood A, Pizzorusso T, Porciatti V, Morales B, Bear MF, Maffei L, Tonegawa S (1999) BDNF
980 regulates the maturation of inhibition and the critical period of plasticity in mouse visual cortex.
981 Cell 98:739-755.
982 Huh D, Paulsson J (2011) Non-genetic heterogeneity from stochastic partitioning at cell division. Nature
983 genetics 43:95-100.
984 Husch A, Paehler M, Fusca D, Paeger L, Kloppenburg P (2009a) Calcium current diversity in
985 physiologically different local interneuron types of the antennal lobe. The Journal of
986 neuroscience : the official journal of the Society for Neuroscience 29:716-726.
987 Husch A, Paehler M, Fusca D, Paeger L, Kloppenburg P (2009b) Distinct electrophysiological properties in
988 subtypes of nonspiking olfactory local interneurons correlate with their cell type-specific Ca2+
989 current profiles. Journal of neurophysiology 102:2834-2845.
990 Hussain A, Ucpunar HK, Zhang M, Loschek LF, Grunwald Kadow IC (2016) Neuropeptides Modulate
991 Female Chemosensory Processing upon Mating in Drosophila. PLoS biology 14:e1002455.
992 Ignell R, Root CM, Birse RT, Wang JW, Nässel DR, Winther AM (2009) Presynaptic peptidergic
993 modulation of olfactory receptor neurons in Drosophila. Proceedings of the National Academy
994 of Sciences of the United States of America 106:13070-13075.
995 Jiang H, Wang Y, Kanost MR (1996) Primary structure of ribosomal proteins S3 and S7 from Manduca
996 sexta. Insect Mol Biol 5:31-38.
997 Kanost MR et al. (2016) Multifaceted biological insights from a draft genome sequence of the tobacco
998 hornworm moth, Manduca sexta. Insect Biochem Mol Biol 76:118-147.
999 Kepecs A, Fishell G (2014) Interneuron cell types are fit to function. Nature 505:318-326.
1000 Ko KI, Root CM, Lindsay SA, Zaninovich OA, Shepherd AK, Wasserman SA, Kim SM, Wang JW (2015)
1001 Starvation promotes concerted modulation of appetitive olfactory behavior via parallel
1002 neuromodulatory circuits. eLife 4.
1003 Lenz O, Xiong J, Nelson MD, Raizen DM, Williams JA (2015) FMRFamide signaling promotes stress-
1004 induced sleep in Drosophila. Brain Behav Immun 47:141-148.
1005 Li H, Horns F, Wu B, Xie Q, Li J, Li T, Luginbuhl DJ, Quake SR, Luo L (2017) Classifying Drosophila Olfactory
1006 Projection Neuron Subtypes by Single-Cell RNA Sequencing. Cell 171:1206-1220 e1222.
1007 Li J, Xiao Y, Zhou W, Wu Z, Zhang R, Xu T (2009) Silence of Synaptotagmin VII inhibits release of dense
1008 core vesicles in PC12 cells. Science in China Series C, Life sciences 52:1156-1163.
1009 Liang X, Holy TE, Taghert PH (2017) A Series of Suppressive Signals within the Drosophila Circadian
1010 Neural Circuit Generates Sequential Daily Outputs. Neuron 94:1173-1189 e1174.

1011 Liu WW, Wilson RI (2013) Glutamate is an inhibitory neurotransmitter in the Drosophila olfactory
1012 system. Proceedings of the National Academy of Sciences of the United States of America
1013 110:10294-10299.
1014 Liu Y, Luo J, Nässel DR (2016) The Drosophila Transcription Factor Dimmed Affects Neuronal Growth and
1015 Differentiation in Multiple Ways Depending on Neuron Type and Developmental Stage. Frontiers
1016 in molecular neuroscience 9:97.
1017 Lizbinski KM, Metheny JD, Bradley SP, Kesari A, Dacks AM (2016) The anatomical basis for modulatory
1018 convergence in the antennal lobe of Manduca sexta. The Journal of comparative neurology
1019 524:1859-1875.
1020 Loesel R, Homberg U (1999) Histamine-immunoreactive neurons in the brain of the cockroach
1021 Leucophaea maderae. Brain research 842:408-418.
1022 Maccaferri G, Lacaille JC (2003) Interneuron Diversity series: Hippocampal interneuron classifications--
1023 making things as simple as possible, not simpler. Trends in neurosciences 26:564-571.
1024 Malun D (1991) Inventory and distribution of synapses of identified uniglomerular projection neurons in
1025 the antennal lobe of Periplaneta americana. The Journal of comparative neurology 305:348-360.
1026 Marder E, Calabrese RL, Nusbaum MP, Trimmer B (1987) Distribution and partial characterization of
1027 FMRFamide-like peptides in the stomatogastric nervous systems of the rock crab, Cancer
1028 borealis, and the spiny lobster, Panulirus interruptus. The Journal of comparative neurology
1029 259:150-163.
1030 Marsat G, Maler L (2010) Neural heterogeneity and efficient population codes for communication
1031 signals. Journal of neurophysiology 104:2543-2555.
1032 Mayer C, Hafemeister C, Bandler RC, Machold R, Brito RB, Jaglin X, Allaway K, Butler A, Fishell G, Satija R
1033 (2018) Developmental diversification of cortical inhibitory interneurons. Nature.
1034 Min S, Chae HS, Jang YH, Choi S, Lee S, Jeong YT, Jones WD, Moon SJ, Kim YJ, Chung J (2016)
1035 Identification of a Peptidergic Pathway Critical to Satiety Responses in Drosophila. Current
1036 biology : CB 26:814-820.
1037 Nässel DR (2018) Substrates for Neuronal Cotransmission With Neuropeptides and Small Molecule
1038 Neurotransmitters in Drosophila. Frontiers in cellular neuroscience 12:83.
1039 Nery S, Fishell G, Corbin JG (2002) The caudal ganglionic eminence is a source of distinct cortical and
1040 subcortical cell populations. Nature neuroscience 5:1279-1287.
1041 Neupert S, Fusca D, Kloppenburg P, Predel R (2018) Analysis of Single Neurons by Perforated Patch
1042 Clamp Recordings and MALDI-TOF Mass Spectrometry. ACS chemical neuroscience 9:2089-2096.
1043 Ng M, Roorda RD, Lima SQ, Zemelman BV, Morcillo P, Miesenbock G (2002) Transmission of olfactory
1044 information between three populations of neurons in the antennal lobe of the fly. Neuron
1045 36:463-474.
1046 Nusbaum MP, Blitz DM, Marder E (2017) Functional consequences of neuropeptide and small-molecule
1047 co-transmission. Nature reviews Neuroscience 18:389-403.
1048 Nusbaum MP, Blitz DM, Swensen AM, Wood D, Marder E (2001) The roles of co-transmission in neural
1049 network modulation. Trends in neurosciences 24:146-154.
1050 Ogawa T, Riera J, Goto T, Sumiyoshi A, Nonaka H, Jerbi K, Bertrand O, Kawashima R (2011) Large-scale
1051 heterogeneous representation of sound attributes in rat primary auditory cortex: from unit
1052 activity to population dynamics. The Journal of neuroscience : the official journal of the Society
1053 for Neuroscience 31:14639-14653.
1054 Okaty BW, Freret ME, Rood BD, Brust RD, Hennessy ML, deBairos D, Kim JC, Cook MN, Dymecki SM
1055 (2015) Multi-Scale Molecular Deconstruction of the Serotonin Neuron System. Neuron 88:774-
1056 791.
1057 Olsen SR, Wilson RI (2008) Lateral presynaptic inhibition mediates gain control in an olfactory circuit.
1058 Nature 452:956-960.

1059 Ormerod KG, Krans JL, Mercier AJ (2015) Cell-selective modulation of the Drosophila neuromuscular
1060 system by a neuropeptide. Journal of neurophysiology 113:1631-1643.
1061 Park D, Taghert PH (2009) Peptidergic neurosecretory cells in insects: organization and control by the
1062 bHLH protein DIMMED. General and comparative endocrinology 162:2-7.
1063 Park D, Veenstra JA, Park JH, Taghert PH (2008a) Mapping peptidergic cells in Drosophila: where DIMM
1064 fits in. PloS one 3:e1896.
1065 Park D, Li P, Dani A, Taghert PH (2014) Peptidergic cell-specific synaptotagmins in Drosophila:
1066 localization to dense-core granules and regulation by the bHLH protein DIMMED. The Journal of
1067 neuroscience : the official journal of the Society for Neuroscience 34:13195-13207.
1068 Park D, Shafer OT, Shepherd SP, Suh H, Trigg JS, Taghert PH (2008b) The Drosophila basic helix-loop-helix
1069 protein DIMMED directly activates PHM, a gene encoding a neuropeptide-amidating enzyme.
1070 Molecular and cellular biology 28:410-421.
1071 Patz S, Grabert J, Gorba T, Wirth MJ, Wahle P (2004) Parvalbumin expression in visual cortical
1072 interneurons depends on neuronal activity and TrkB ligands during an Early period of postnatal
1073 development. Cerebral cortex 14:342-351.
1074 Peng H, Ruan Z, Long F, Simpson JH, Myers EW (2010) V3D enables real-time 3D visualization and
1075 quantitative analysis of large-scale biological image data sets. Nat Biotechnol 28:348-353.
1076 Pitkow X, Meister M (2012) Decorrelation and efficient coding by retinal ganglion cells. Nature
1077 neuroscience 15:628-635.
1078 Pratt GE, Farnsworth DE, Fok KF, Siegel NR, McCormack AL, Shabanowitz J, Hunt DF, Feyereisen R (1991)
1079 Identity of a second type of allatostatin from cockroach brains: an octadecapeptide amide with a
1080 tyrosine-rich address sequence. Proceedings of the National Academy of Sciences of the United
1081 States of America 88:2412-2416.
1082 Predel R, Rapus J, Eckert M (2001) Myoinhibitory neuropeptides in the American cockroach. Peptides
1083 22:199-208.
1084 Raj A, van Oudenaarden A (2008) Nature, nurture, or chance: stochastic gene expression and its
1085 consequences. Cell 135:216-226.
1086 Reichwald K, Unnithan GC, Davis NT, Agricola H, Feyereisen R (1994) Expression of the allatostatin gene
1087 in endocrine cells of the cockroach midgut. Proceedings of the National Academy of Sciences of
1088 the United States of America 91:11894-11898.
1089 Reisenman CE, Dacks AM, Hildebrand JG (2011) Local interneuron diversity in the primary olfactory
1090 center of the moth Manduca sexta. Journal of comparative physiology A, Neuroethology,
1091 sensory, neural, and behavioral physiology 197:653-665.
1092 Root CM, Masuyama K, Green DS, Enell LE, Nässel DR, Lee CH, Wang JW (2008) A presynaptic gain
1093 control mechanism fine-tunes olfactory behavior. Neuron 59:311-321.
1094 Salio C, Lossi L, Ferrini F, Merighi A (2006) Neuropeptides as synaptic transmitters. Cell Tissue Res
1095 326:583-598.
1096 Saraswati S, Adolfsen B, Littleton JT (2007) Characterization of the role of the Synaptotagmin family as
1097 calcium sensors in facilitation and asynchronous neurotransmitter release. Proceedings of the
1098 National Academy of Sciences of the United States of America 104:14122-14127.
1099 Schachtner J, Trosowski B, D'Hanis W, Stubner S, Homberg U (2004) Development and steroid regulation
1100 of RFamide immunoreactivity in antennal-lobe neurons of the sphinx moth Manduca sexta. The
1101 Journal of experimental biology 207:2389-2400.
1102 Schafer S, Bicker G (1986) Distribution of GABA-like immunoreactivity in the brain of the honeybee. The
1103 Journal of comparative neurology 246:287-300.
1104 Seidel C, Bicker G (1997) Colocalization of NADPH-diaphorase and GABA-immunoreactivity in the
1105 olfactory and visual system of the locust. Brain research 769:273-280.

1106 Siju KP, Reifenrath A, Scheiblich H, Neupert S, Predel R, Hansson BS, Schachtner J, Ignell R (2013)
1107 Neuropeptides in the antennal lobe of the yellow fever mosquito, Aedes aegypti. The Journal of
1108 comparative neurology.
1109 Skaer NJ, Nässel DR, Maddrell SH, Tublitz NJ (2002) Neurochemical fine tuning of a peripheral tissue:
1110 peptidergic and aminergic regulation of fluid secretion by Malpighian tubules in the tobacco
1111 hawkmoth M. sexta. The Journal of experimental biology 205:1869-1880.
1112 Stratmann J, Thor S (2017) Neuronal cell fate specification by the molecular convergence of different
1113 spatio-temporal cues on a common initiator terminal selector gene. PLoS genetics 13:e1006729.
1114 Sun X, Fonta C, Masson C (1993) Odour quality processing by bee antennal lobe interneurones. Chemical
1115 senses 18:355-377.
1116 Sweeney LB, Bikoff JB, Gabitto MI, Brenner-Morton S, Baek M, Yang JH, Tabak EG, Dasen JS, Kintner CR,
1117 Jessell TM (2018) Origin and Segmental Diversity of Spinal Inhibitory Interneurons. Neuron
1118 97:341-355 e343.
1119 Teal PE (2002) Effects of allatotropin and allatostatin on in vitro production of juvenile hormones by the
1120 corpora allata of virgin females of the moths of Heliothis virescens and Manduca sexta. Peptides
1121 23:663-669.
1122 Tritsch NX, Granger AJ, Sabatini BL (2016) Mechanisms and functions of GABA co-release. Nature
1123 reviews Neuroscience 17:139-145.
1124 Utz S, Schachtner J (2005) Development of A-type allatostatin immunoreactivity in antennal lobe
1125 neurons of the sphinx moth Manduca sexta. Cell Tissue Res 320:149-162.
1126 Utz S, Huetteroth W, Vomel M, Schachtner J (2008) Mas-allatotropin in the developing antennal lobe of
1127 the sphinx moth Manduca sexta: distribution, time course, developmental regulation, and
1128 colocalization with other neuropeptides. Developmental neurobiology 68:123-142.
1129 Utz S, Huetteroth W, Wegener C, Kahnt J, Predel R, Schachtner J (2007) Direct peptide profiling of lateral
1130 cell groups of the antennal lobes of Manduca sexta reveals specific composition and changes in
1131 neuropeptide expression during development. Developmental neurobiology 67:764-777.
1132 Veenstra JA, Hagedorn HH (1995) Isolation of two AKH-related peptides from cicadas. Archives of insect
1133 biochemistry and physiology 29:391-396.
1134 Wichterle H, Turnbull DH, Nery S, Fishell G, Alvarez-Buylla A (2001) In utero fate mapping reveals distinct
1135 migratory pathways and fates of neurons born in the mammalian basal forebrain. Development
1136 128:3759-3771.
1137 Wilson RI (2013) Early olfactory processing in Drosophila: mechanisms and principles. Annual review of
1138 neuroscience 36:217-241.
1139 Wilson RI, Laurent G (2005) Role of GABAergic inhibition in shaping odor-evoked spatiotemporal
1140 patterns in the Drosophila antennal lobe. The Journal of neuroscience : the official journal of the
1141 Society for Neuroscience 25:9069-9079.
1142 Witten JL, Truman JW (1996) Developmental plasticity of neuropeptide expression in motoneurons of
1143 the moth, Manduca sexta: steroid hormone regulation. Journal of neurobiology 29:99-114.
1144 Yapici N, Kim YJ, Ribeiro C, Dickson BJ (2008) A receptor that mediates the post-mating switch in
1145 Drosophila reproductive behaviour. Nature 451:33-37.
1146 Yavorska I, Wehr M (2016) Somatostatin-Expressing Inhibitory Interneurons in Cortical Circuits. Frontiers
1147 in neural circuits 10:76.
1148
1149

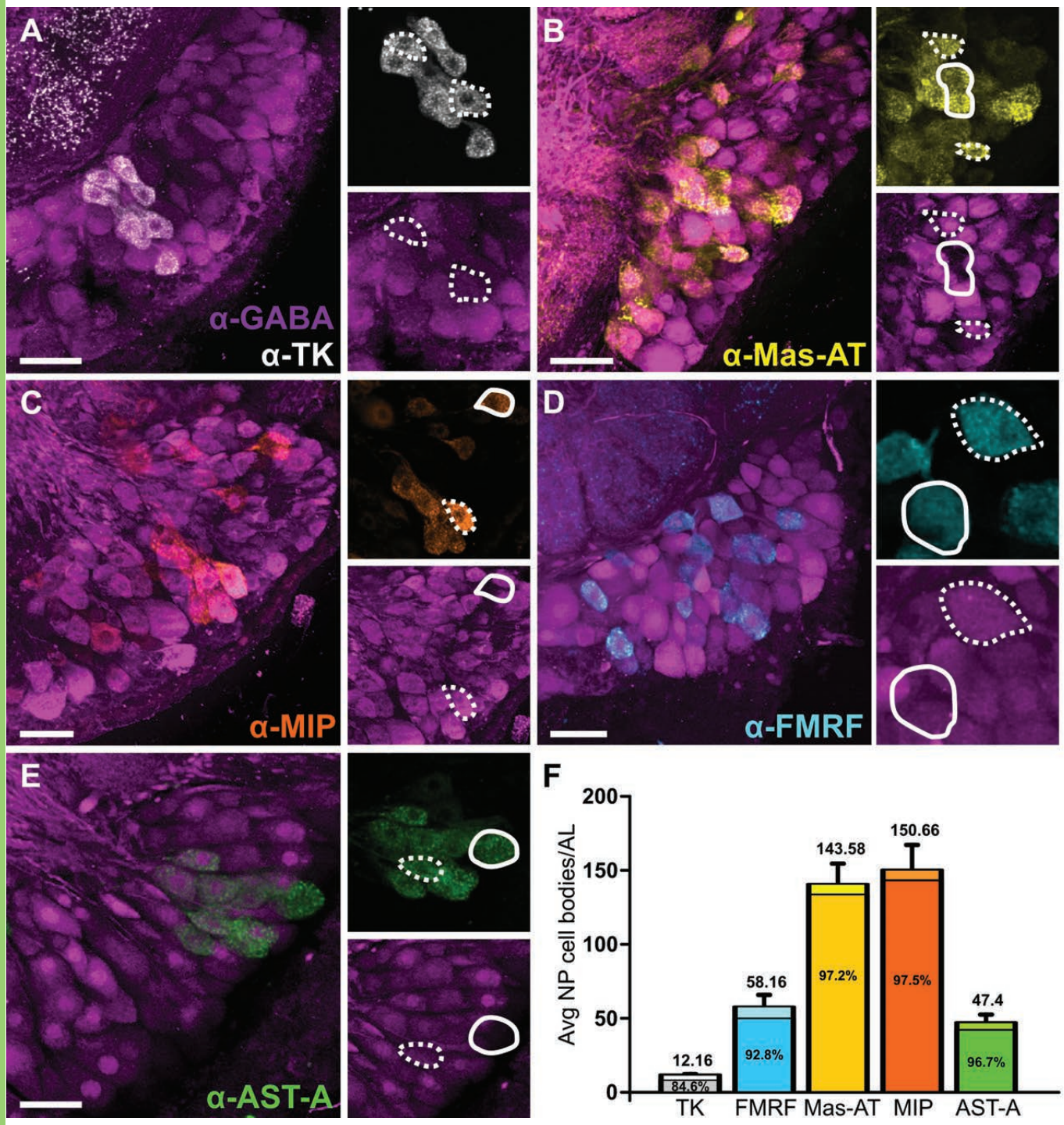

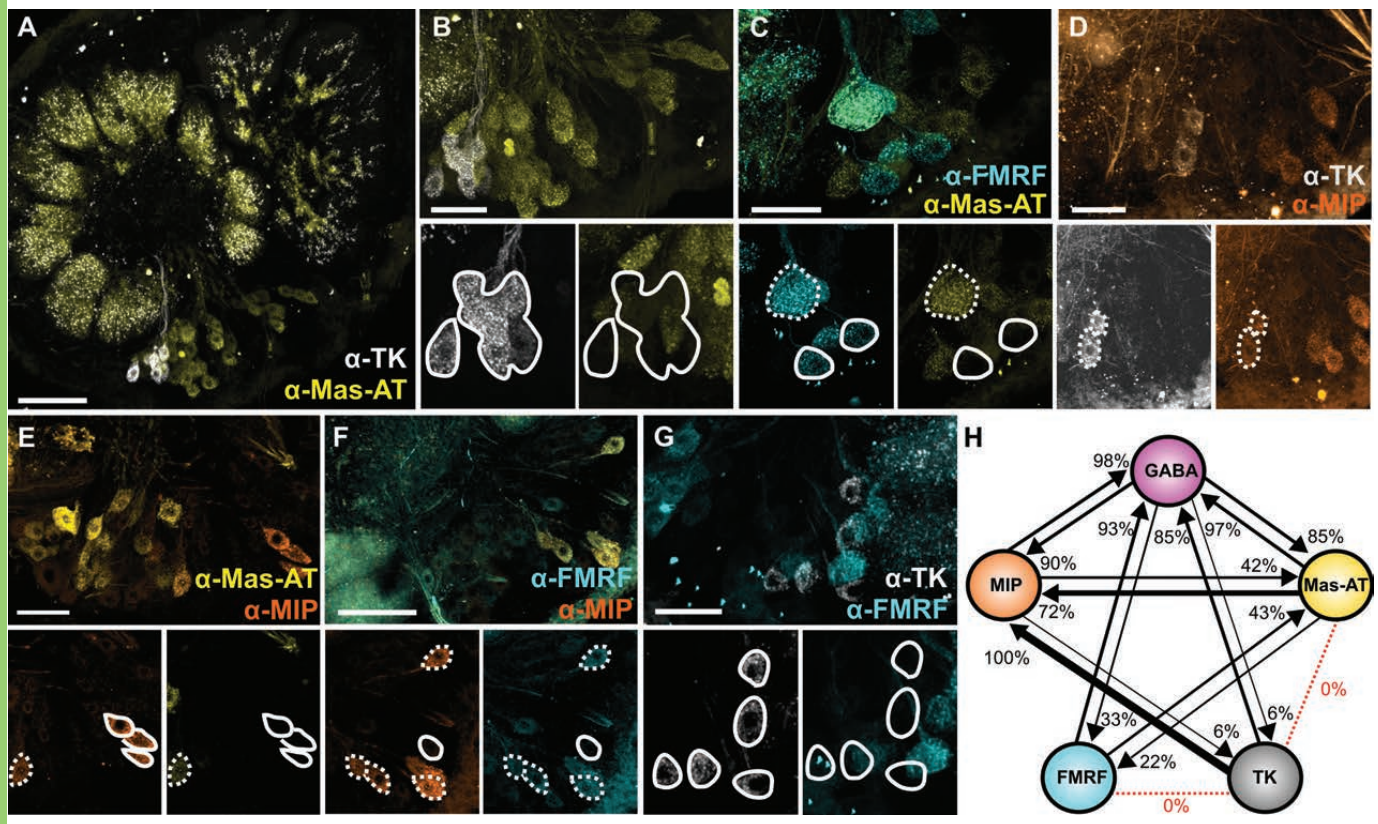

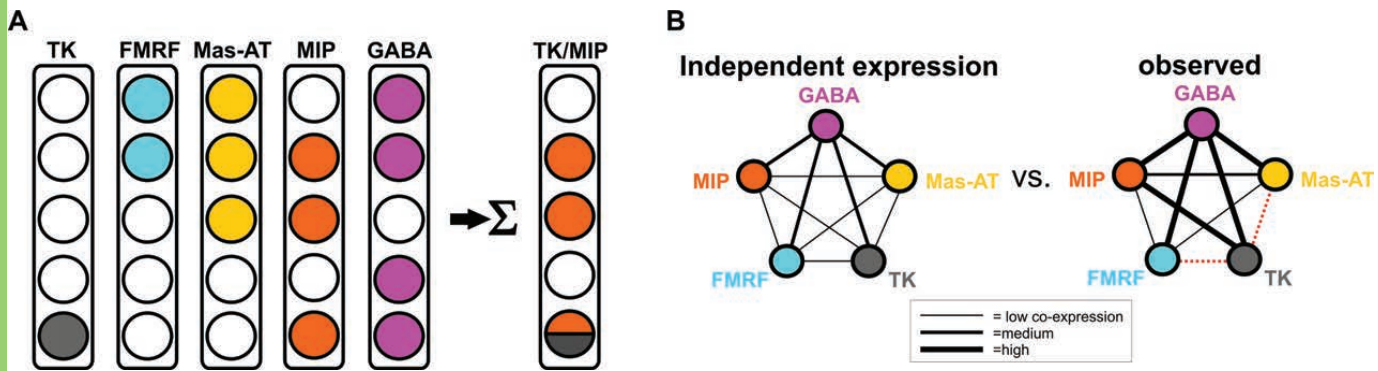

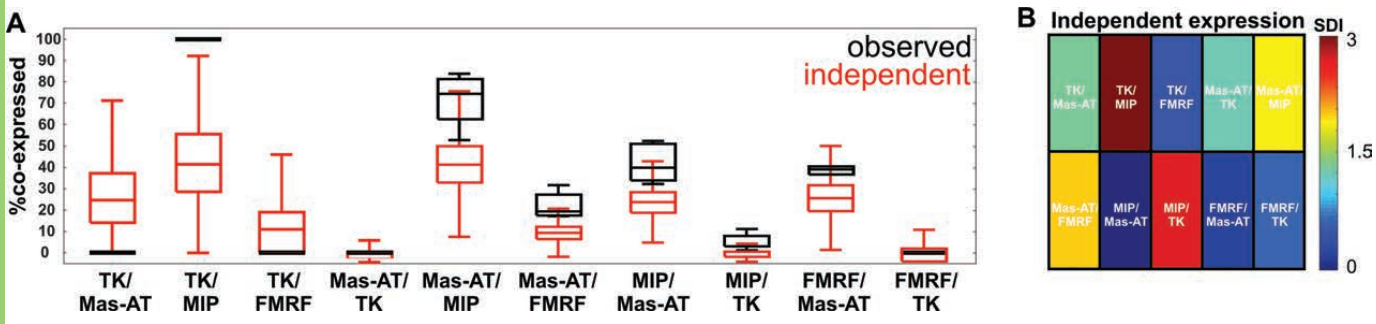

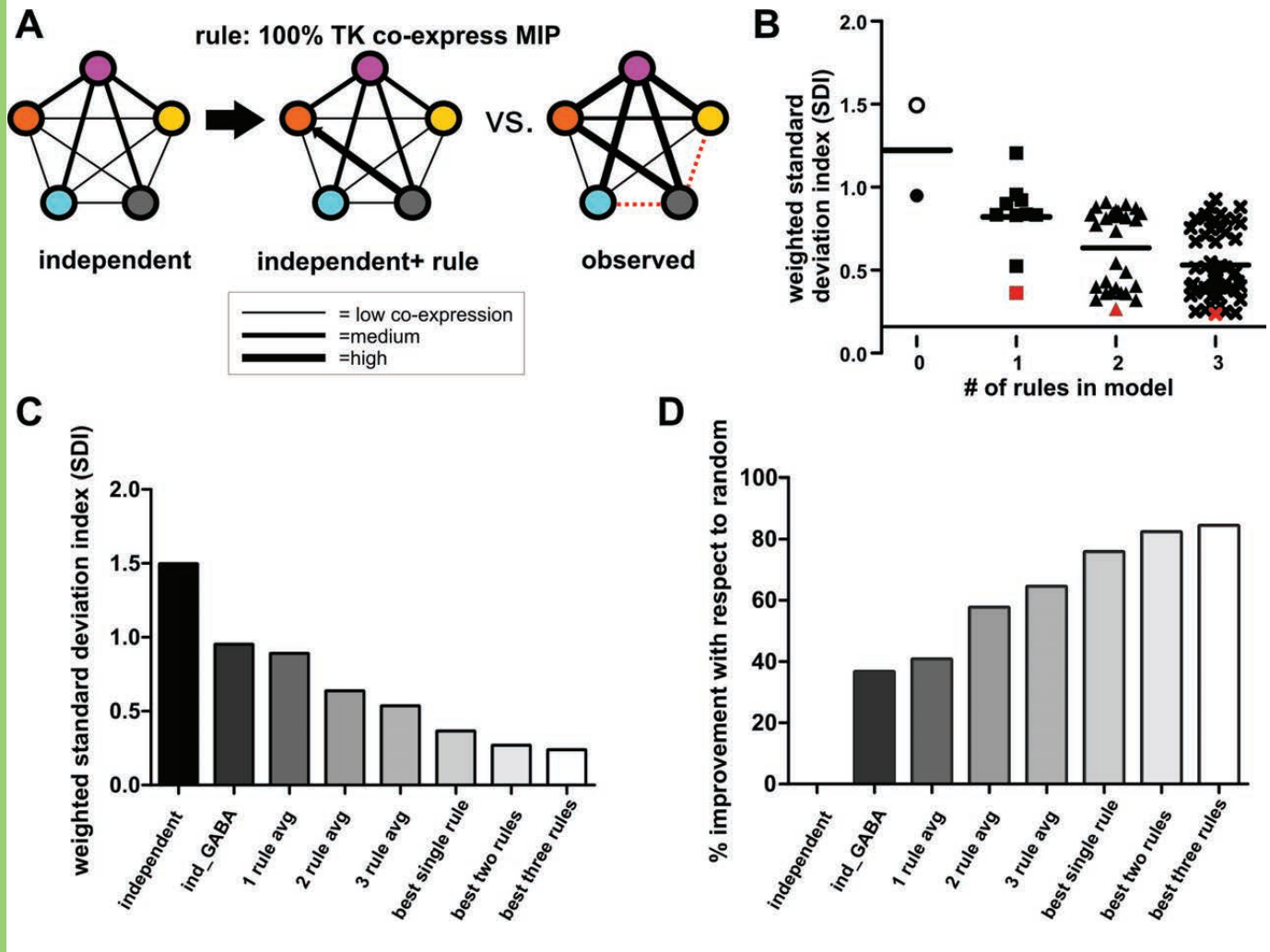

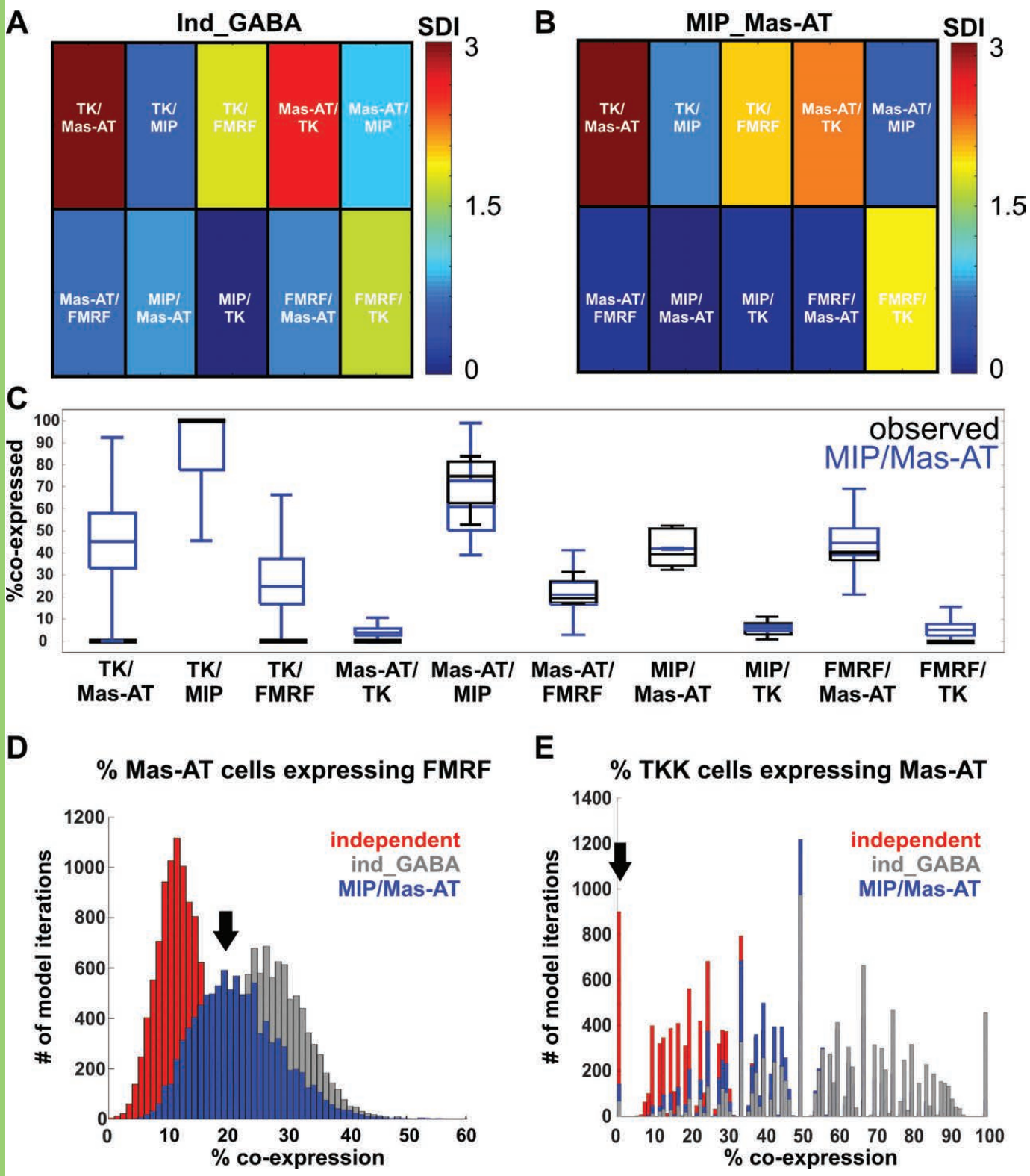

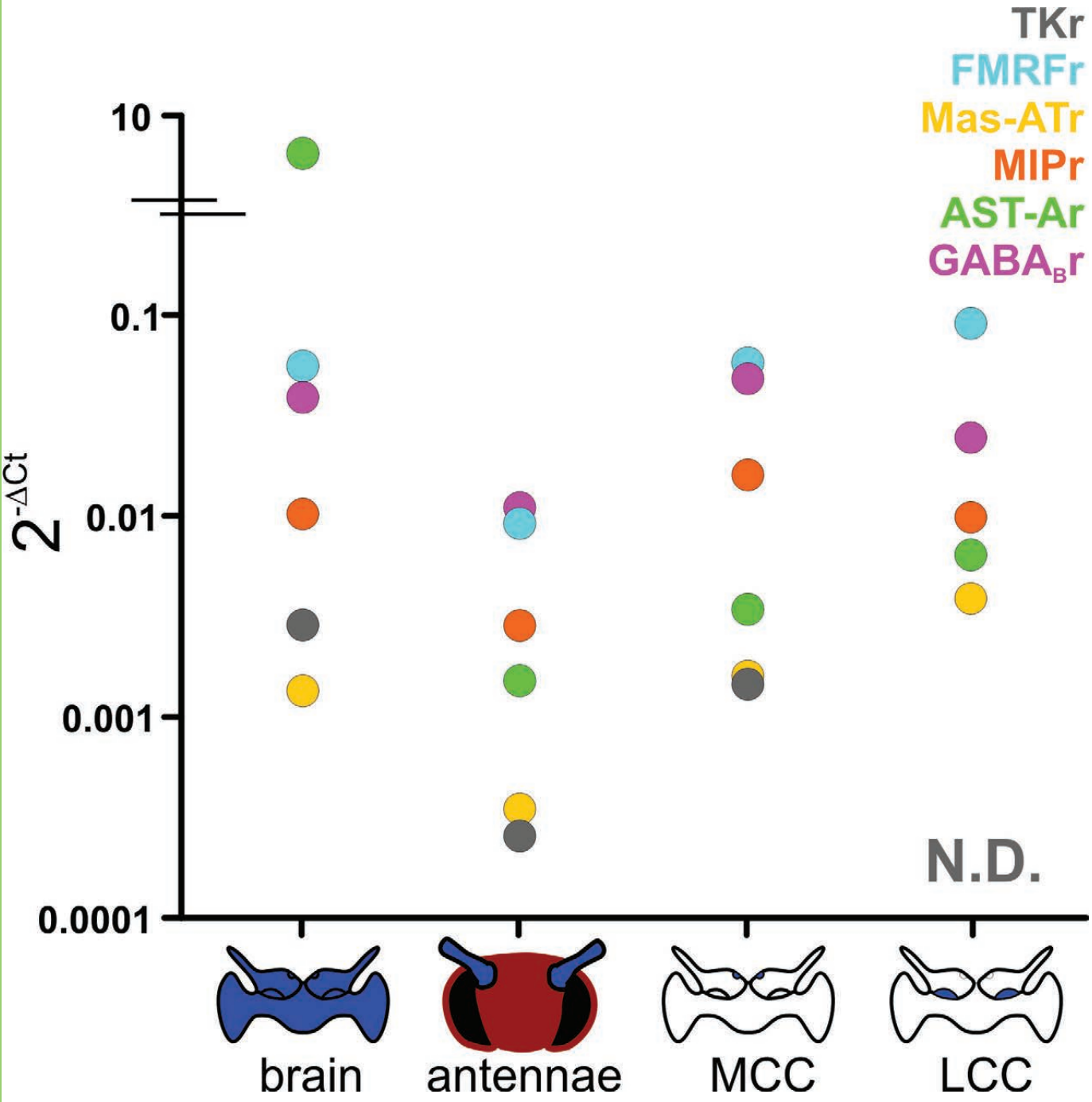

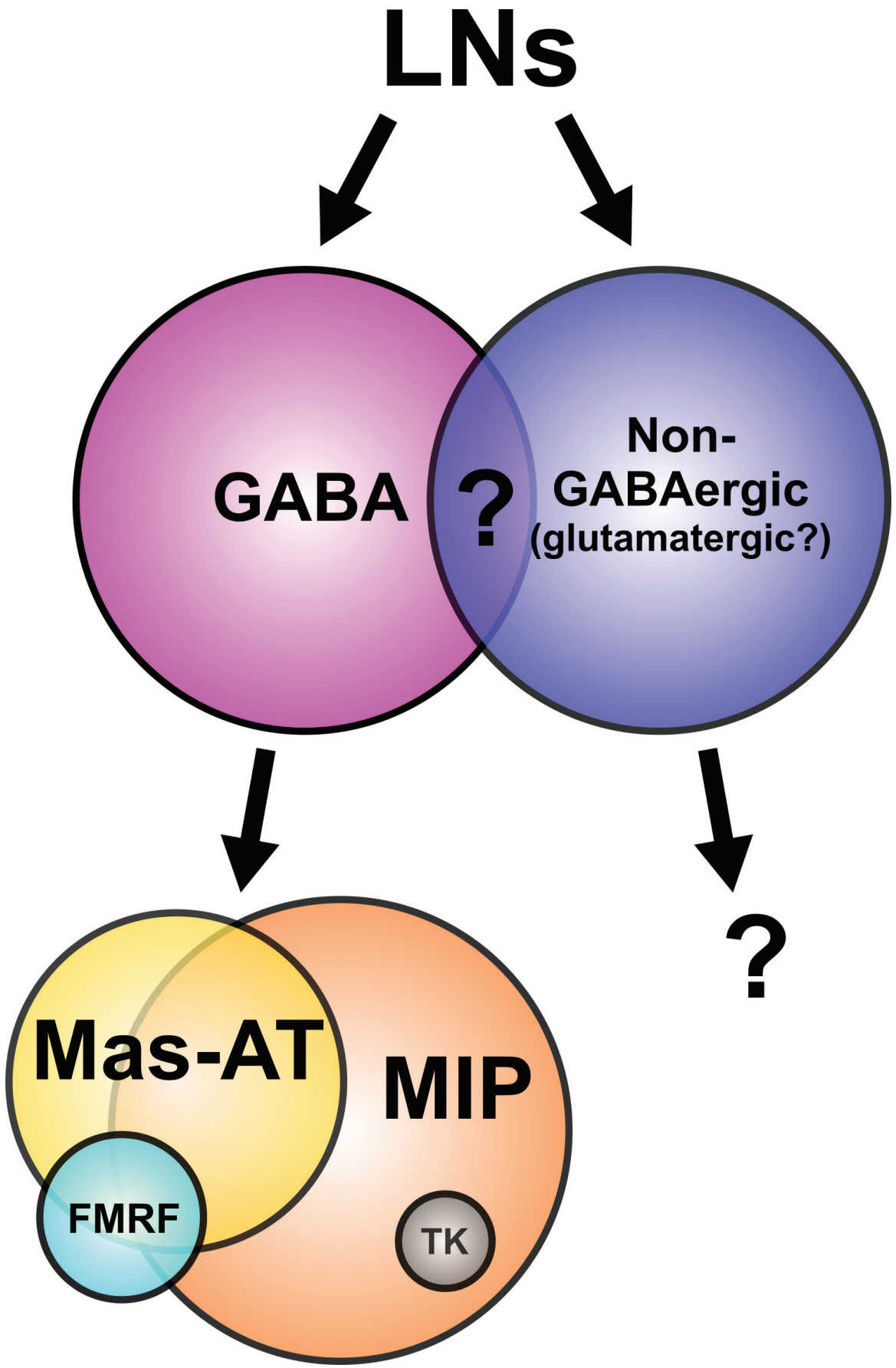

Table 1: Neuropeptide cell body totals and % co-expression with GABA

Neuropeptide	Avg # of cell bodies in lateral cell cluster	% co-expression with GABA
TK	12.16 ± 0.55	84.6%
FMRF	58.16 ± 17.48	92.8%
Mas-AT	143.58± 24.38	97.2%
MIP	150.66 ± 16.79	97.5%
AST-A	47.4 ± 12.83	96.7%

Table 2: BLAST results for neuropeptide receptor primer design and primer sequences

Receptor	Accession # of sequence for forward BLAST and origin species	Returned *M. sexta* subject sequence ID and E value	Accession # of Reverse BLAST top hit	Primer sequences		Annealing temp. (Celsius)
				Forward	Reverse	
TKr	AAA28722.1 (*D. melanogaster*)	Msex2.00568-RA scaffold00007:996602-1079056(+) JH668285.1 E value: e-103	NP_001127749.1 (*Bombyx mori*)	ACAGGTACGTGGCGATAGTG	AGCTGGCACACCAAACAGTA	58.3
FMRFr	AHN57950.1 (*D. melanogaster*)	Msex2.13475-RA scaffold01034:41471-49046(+) JH669301.1 E value: 2e-77	NP_001037007.1 (*Bombyx mori*)	ACCGTGCTCATCCTTACCTC	TGCGGACACACGTGATAGTA	58.3
ASTr	AAG22404.3 (*D. melanogaster*)	Msex2.08175-RB scaffold00218:172215-185483(-) JH668496.1 E value: e-100	ACJ06649.1 (*Spodoptera littoralis*)	ATCTGGCCGTAGCTGATCTT	GCATTACATAATCCGTTGCG	58.3
MIPr	NP_001108346.1 (*Bombyx mori*)	Msex2.12746-RA scaffold00798:532-18804(+) JH669075.1 E value: e-139	AGE92037.1 (*Spodoptera litura*)	GGGTTCAGGGTACTGTTCGT	GAACAGGAGCACATTCAGGA	58.3
Mas-ATr	ADX66344.1 (*M. sexta* Horodyski et al 2011)	JH668656.1	N/A	TTCCTTGGAGACGTGCTGT	ACTTGAACTTGAGCGGG	52
$GABA_B$-R1	HG004164.1 (*Heliothis virescens)* (at European Nucleotide Archive)	Msex2.03321-RA scaffold00068:510618-566612(-) JH668346.1 E value: 0.0	XM_013339859.1 (*Amyelois transitella*)	TATTTCGGGAATGACTTCTG	TCAATATCATATCCGGCTTC	58.3
RPs3	U12708 (*M. sexta*) (Jiang et al 1996)	JH668297.1	N/A	CATGATCCACTCCGGTGAC	GACCTTAATTCCGAGCACTCC	58.3
vGLUT	FBgn0031424 (*D. melanogaster*) (at FlyBase)	JH668481 E value: 5e-18	XM_014627996.1 (Dinoponera quadriceps)	GACCACGACTAATGTGCGGA	CATTGAGTTGACGATCGGCG	58.3

Table 3: Cq values for all receptors and RpS3 from RT-qPCR

		ANTa	ANTb	ANTc	Ba	Bb	Bc	Ma	Mb	Mc	La	Lb	Lc	genomic
TKr	RT	0	34.1	34.5	31.36	35.35	29.63	38.51	32.18	34.03	39	0	37.59	24.09
	RT-	0	0	0	0	0	0	0	0	0	0	0	0	0 (NTC)
Mas-ATr	RT	35.72	33.65	33.41	32.28	37.32	31.26	39.8	32.42	33.55	35.77	37.6	36.29	30.24
	RT-	0	0	0	0	0	0	0	0	0	0	0	0	39.48 (NTC)
FMRFr	RT	32.43	29.04	29.1	26.56	31.14	25.95	33.01	27.53	28.03	31.57	32.22	30.89	24.85
	RT-	0	0	0	0	0	0	0	0	0	0	0	0	0 (NTC)
MIPr	RT	33.91	31.03	30.69	29.55	33.31	27.94	34.94	28.92	30.15	34.97	35.73	33.12	23.86
	RT-	0	0	0	0	0	0	0	0	0	0	0	0	0 (NTC)
AST-Ar	RT	37.28	32.23	31.23	29.26	23.63	28.17	37.39	31.19	32.39	35.43	37.35	35.14	25.61
	RT-	0	0	0	0	0	0	0	0	0	0	0	0	0 (NTC)
$GABA_B$	RT	32.21	29.09	28.62	27.91	31.17	25.97	33.48	27.26	28.51	33.26	35.51	31.97	23.72
	RT-	0	0	0	0	0	0	0	0	0	0	0	0	0 (NTC)
vGlut	RT	x	x	x	24.43	28.40	23.21	x	x	x	32.60	0	31.96	24.82
	RT-	x	x	x	0	0	0	x	x	x	0	0	0	0 (NTC)
RpS3	RT	25.61	22.49	22.16	22.91	26.65	21.41	28.89	23.16	24.04	28.93	28.6	26.04	24.18
	RT-	0	0	0	0	0	0	0	0	0	0	0	0	0 (NTC)
RpS3 (at 52˚C)	RT	24.54	21.85	21.87	23.18	27.04	21.31	28	23.21	24.18	26.68	28.03	25.23	18.29
	RT-	4.41	0	0	39	37.27	0	37.2	5.13	28.94	36.16	38.98	0	5.23 (NTC)